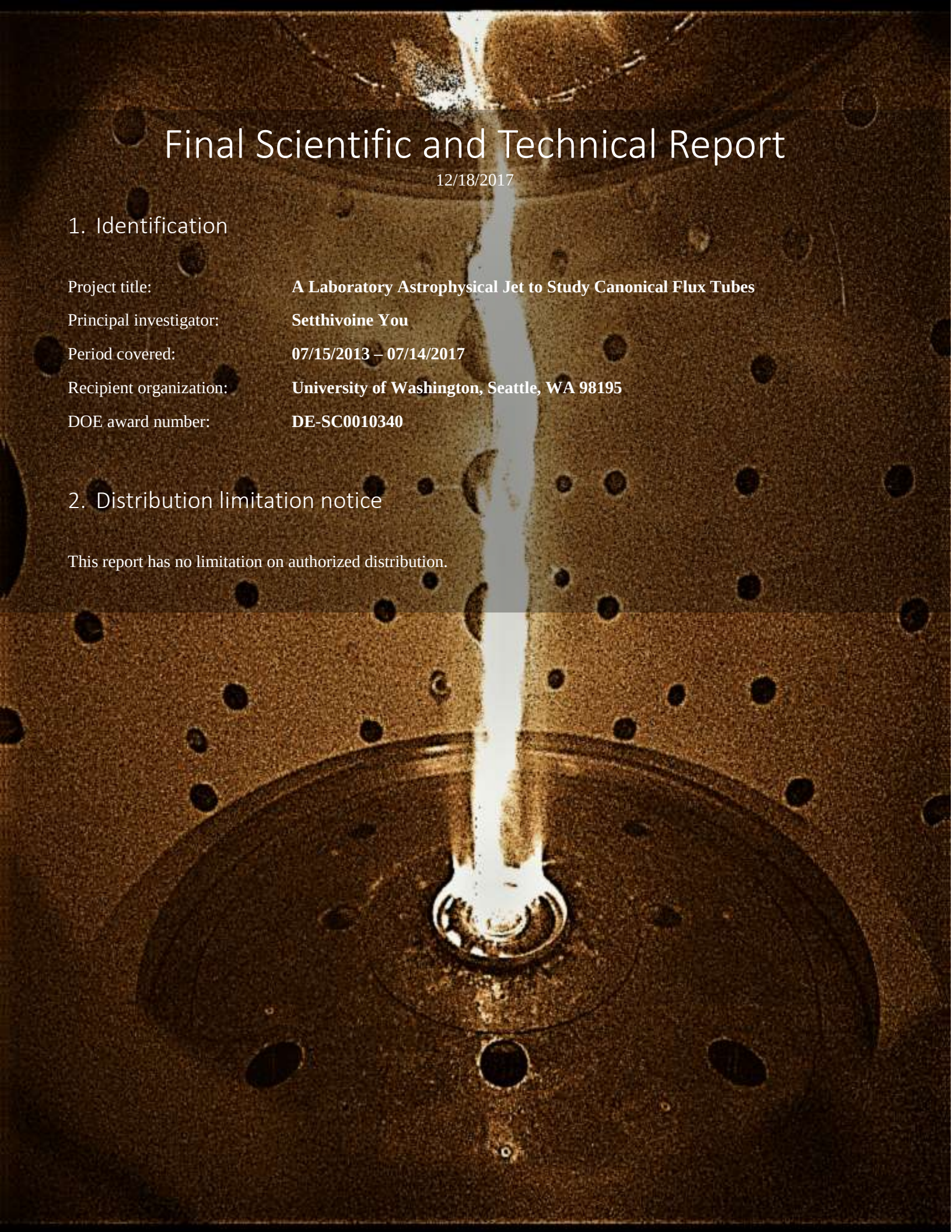

Final Scientific and Technical Report

12/18/2017

1. Identification

Project title:	**A Laboratory Astrophysical Jet to Study Canonical Flux Tubes**
Principal investigator:	**Setthivoine You**
Period covered:	**07/15/2013 – 07/14/2017**
Recipient organization:	**University of Washington, Seattle, WA 98195**
DOE award number:	**DE-SC0010340**

2. Distribution limitation notice

This report has no limitation on authorized distribution.

Table of Contents

Cover page image: high speed photograph of laboratory astrophysical jet produced in the Mochi.LabJet experiment (shot #6903 at 57 μs).

3. Executive summary

Understanding the interaction between plasma flows and magnetic fields remains a fundamental problem in plasma physics, with important applications to astrophysics, fusion energy, and advanced space propulsion.

For example, flows are of primary importance in astrophysical jets even if it is not fully understood how jets become so long without becoming unstable. Theories for the origin of magnetic fields in the cosmos rely on flowing charged fluids that should generate magnetic fields, yet this remains to be demonstrated experimentally. Fusion energy reactors can be made smaller with flows that improve stability and confinement. Advanced space propulsion could be more efficient with collimated and stable plasma flows through magnetic nozzles but must eventually detach from the nozzle. In all these cases, there appears to be a spontaneous emergence of flowing and/or magnetic structures, suggesting a form of self-organization in plasmas. Beyond satisfying simple intellectual curiosity, understanding plasma self-organization could enable the development of methods to control plasma structures for fusion energy, space propulsion, and other applications.

The research project has therefore built a theory and an experiment to investigate the interaction between magnetic fields and plasma flows. The theory is called canonical field theory for short, and the experiment is called Mochi after a rice cake filled with surprising, yet delicious fillings[1].

The theory generalizes earlier ones to more realistic regimes, including relativistic and fully kinetic regimes. It unifies all the existing equations of plasma physics into a single framework. It predicts how flows can be generated from magnetic fields untwisting or vice-versa. It suggests that the twistedness of magnetic fields is coupled to the twistedness of flows. It suggests that the collimation of astrophysical jets could be the result of flow vorticities dominating magnetic fields far from the footpoints. The theory compares well to existing experimental results from other laboratories but requires more testing with experiments and more investigation into the implications and promises. Related theoretical work investigated a novel coupling between sausage and kink instabilities, suggesting that magnetic flux tubes with electrical current can detach with this cascade of instabilities. The canonical field theory was used to analyse the plasma detachment results from a magnetoplasma rocket experiment, predicting a return flow near the edge of the plume of the thruster.

The Mochi experiment is a new, flexible, pulsed-power facility designed to investigate how plasma flows interact with magnetic fields. At present, the investigation concentrates on a cylindrical geometry. In future, the plan is to produce toroidal configurations with the same apparatus. The chamber is spherical with numerous ports, so plasma sources can be mounted at different locations and still use the same set of diagnostics. The primary plasma source is the LabJet gun, designed to simulate an astrophysical jet in the laboratory. The unique configuration mimics an accretion disk around a central star with three concentric, planar electrodes, each with azimuthally symmetric gas slits, threaded by a vacuum magnetic field. The setup successfully produces record long, collimated, stable magnetized plasma jets. The results demonstrate for the first time that helical shear flows can stabilize highly-collimated, very long aspect-ratio, current-carrying magnetic flux tubes. Detailed observations also show that the jet has a double-helix magnetic structure that results from self-organization of the plasma into an elongated relaxed state. This magnetic structure resembles some real astrophysical jets that have a double-helix structure.

[1] A “back-cronym” was later defined: Measurements Of Canonical Helicity Injection.

The project began in Jul. 2013 with two PhD students, with 6 MS students joining the group along the way. Most of the experiment was entirely built in-house: it took four years to design and build the plasma gun, the five pulsed-power capacitor banks, the fast gas puff valves, the control & data acquisition setup, and the diagnostics. The spherical vacuum chamber took a year from order to delivery. The experiment achieved first plasma in Nov. 2015. The commissioning phase was nominally completed in Aug. 2016, after resolving critical issues, with a first operational campaign lasting until Nov. 2016 to determine the first plasma parameters while implementing the first diagnostics (current, voltage, interferometer). The results from this campaign informed an upgrade of the plasma gun that resulted in a ten-fold improvement in plasma jet lifetime at the same parameters, leading into the second operational campaign between Dec. 2016 and Mar. 2017. During this campaign, the second set of diagnostics were constructed (magnetic probe arrays and multi-chord ion Doppler spectroscopy) and completed in Apr. 2017. The third operational campaign then collected the most complete set of data between until Jul. 2017. Analysis of this data set is ongoing as of this writing.

The project was terminated one year before the expected end because the PI was denied tenure by a veto from the new Dean of the College of Engineering over the unanimous favorable vote by the Department faculty. The project resulted to-date in 5 publications (with 5 more under review and under preparation), 2 PhD dissertations (1 due June 2018), 4 MS dissertations, 22 international conference presentations, 11 invited talks, 8 contributed talks, 3 articles in international public outreach magazines (1 under preparation), and a Microsoft video on the use of Surface tablet computers in research and teaching. The students have found employment in experimental plasma physics or related employment, at the Lawrence Livermore National Laboratory, the Max-Planck Institute with Wendelstein-7X in Germany, Eagle Harbor Technologies, and one is pending a postdoc position in experimental plasma physics in the United States. The PI left the University of Washington on 15th June 2017, is currently a Visiting Associate Professor at the University of Tokyo, remotely supervises the final PhD student towards a graduation expected in June 2018, and bears the costs of the final 5 project-related publications from personal funds.

4. Comparisons of actual accomplishments with the goals and objectives of the project

4.1. Goals and objectives

The main scientific goal was defined in the Executive Summary of the Project Narrative of the supported proposal:

> *"the objective of the research program outlined in this CAREER proposal is to simulate a magnetically driven jet launched by an accretion disk in a laboratory experiment. […] the aim is to test the hypothesis that magnetically-driven astrophysical jets can become long and collimated without becoming unstable thanks to a combination of strong shear flows and a dynamic reduction in magnetic helicity."*

The project separated the scientific goal into two objectives: building the proposed experimental setup (Section 3 of the Project Narrative), and performing the proposed research (Section 4 of the Project Narrative). The work to build the proposed experimental setup was broken down into the following elements (numbering loosely taken from Section 3 of the Project Narrative):

- *3.1 Magnetized plasma gun design*
  - *3.1.1 Electrode configuration*
  - *3.1.2 Gas source configuration*
  - *3.1.3 Design parameters*
- *3.2 Vacuum chamber*
- *3.3 Power supplies*
- *3.4 Diagnostics*
  - *3.4.1 Magnetic probe array*
  - *3.4.2 Multichannel Passive Optical Spectroscopy*
  - *3.4.3 Fast Ion Gauge*
  - *3.4.4 Interferometer*
  - *3.4.5 Triggers and Data Acquisition*
- *3.5 Vector tomographic reconstruction of spectroscopy measurements*

The proposed research consisted of investigating the stability of the jet with the following elements (numbering loosely taken from Section 4 of the Project Narrative):

4.1. *"The proposed astrophysical jet experiment is ideal for investigating […] whether the boundary conditions can be set up such that magnetic helicity can be continuously converted to kinetic helicity such that q<1 as the column lengthens and therefore remains stable to the Kruskal-Shafranov kink instability."*

4.2. *"modifying the enthalpy at the boundaries such that when the canonical helicity injection is below the 1/S* threshold, it will channel helicity more into the kinetic component rather than the magnetic component of the astrophysical jet."*

4.3. *Analytically and numerically investigate the stability space of current-carrying magnetic flux tubes for arbitrary boundary conditions at the footpoints.*

4.4. *Experimentally investigate the same stability space: "The proposed experiment will be able to explore this space to map out the stability regions and compare to Eq. (2) [the generalized analytical kink and sausage stability criterion]. Comparisons with stability criterion of single line-tied columns will also be done."*

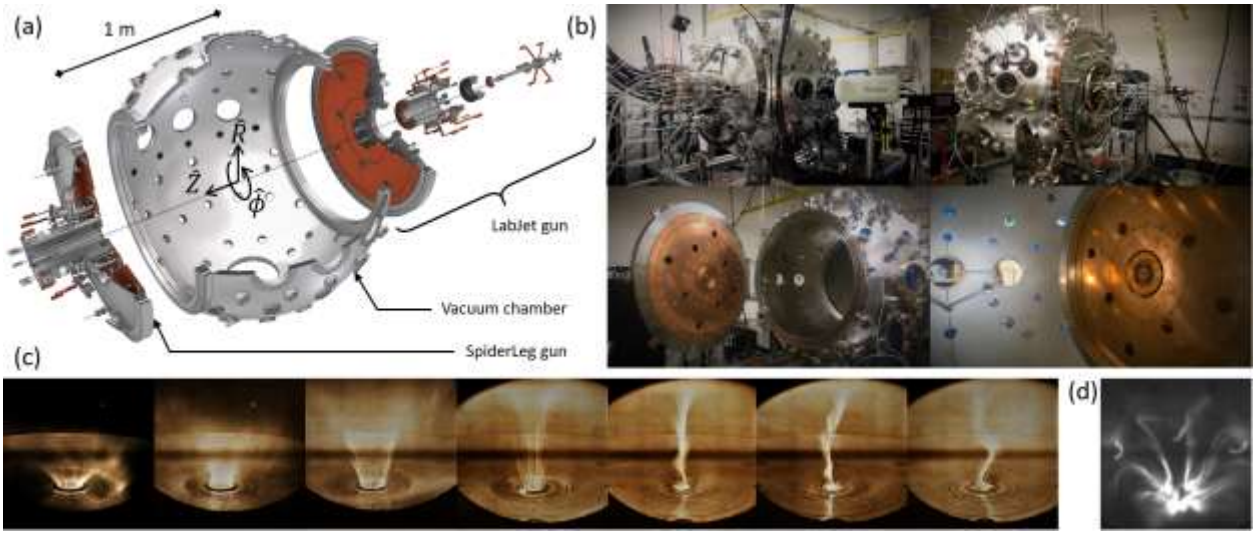

Figure 1. The Mochi facility: (a) schematic showing the mounting of the LabJet gun opposite the SpiderLeg gun on the spherical vacuum chamber. The numerous viewports generally point radially to the center of the sphere, except for several diagnostic ports that point to the Z-axis of the chamber within an azimuthal plane. The cutouts in the LabJet gun provide access to the viewports behind the gun, there are none behind the SpiderLeg gun; (b) photographs of the apparatus showing the LabJet gun (top left), the SpiderLeg gun (top right), the hinged door with the LabJet gun and the tungsten coated SpiderLeg gun in the background (bottom left), the typical high-speed camera view of the LabJet gun (bottom right); (c) Typical plasma jets formed from the LabJet gun during the first operational campaign showing azimuthally-symmetric tubes forming, lengthening, collimating and undergoing instabilities; (d) Early plasma discharge in the SpiderLeg gun showing discrete, kinked, current-carrying magnetic flux tubes linking the gas holes.

The project thus wanted to address the following scientific questions (Executive Summary of the Project Narrative):

a. *Can the appropriate enthalpy boundary conditions establish sufficient axial and azimuthal shear flow to sustain the singly line-tied collimated jet over very long aspect ratios?*
b. *Does magnetic helicity get converted to helical flows as predicted by the relative canonical helicity transport theory?*
c. *Can a shear flow-drive with enthalpy injection (analogous to current-drive by helicity injection) be applied to a toroidal configuration as predicted by the theory?*
d. *Does the intuition of twists, writhes and links familiar from magnetic flux tube evolution be transposed to canonical flux tube evolution?*

For comparison, the actual accomplishments are separately described in the experimental sub-section 4.2 and the theoretical sub-sections 4.3. Sub-section 4.4 describes unexpected, interesting, scientific results. Sub-section 4.5 describes incomplete or obsolete tasks in light of new results. Section 5 summarizes the project activities for the entire period of funding. Section 6 lists the products developed under the award. The following list of accomplishments refer to some of the delivered products of Section 6 with square brackets, e.g. Ref. [Product 6.1.1] to the 1st peer-reviewed paper listed in sub-section 6.1.

4.2. Experimental accomplishments

The project has successfully built the Mochi experiment (Fig. 1), which in the LabJet configuration mimicks a magnetically-driven astrophysical jet (see Section 5 for a summary of the project activities and Ref. [Product developed under award 6.2.1] for details). The apparatus is the first in the world to produce long (aspect-ratio of ~30:1), fully collimated jets with an axial magnetic field and axial currents that remain stable

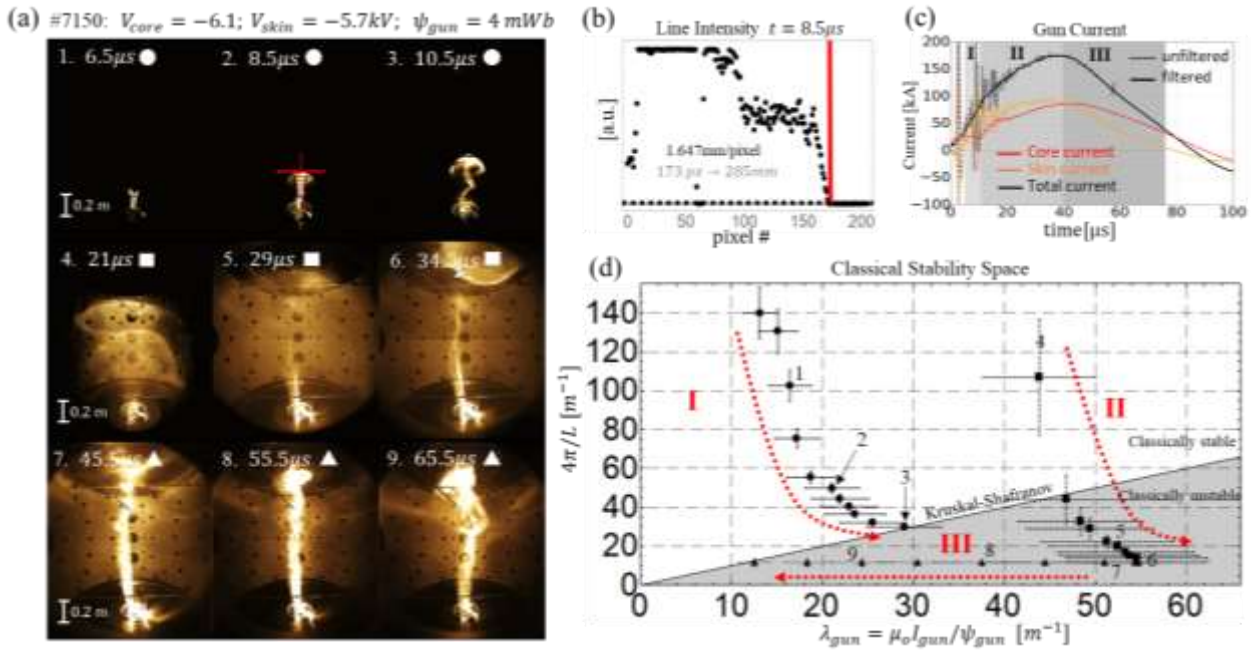

Figure 2. Evolution of shot #7150. (a) High speed camera images reveal three distinct phases in jet formation: I) A narrow collimated jet that goes kink unstable. II) A diffuse lengthening jet. III)A long, stable, collimated jet. (b) line intensity profile at $t = 8.5\mu s$. Jet length is calculated from where the intensity increases 10% above the background. Known gun features provide a reference length in pixels. (c) Gun current traces measured using Rogowski coils. (d) Jet evolution in k, λ stability space. The initial jet goes unstable upon reaching the Kruskal-Shafranov kink condition. The secondary jet forms in stable space, but crosses into classically unstable space as it lengthens and current ramps up. The long, collimated jet remains stable for $\gtrsim 35\mu s$ as current decreases to zero.

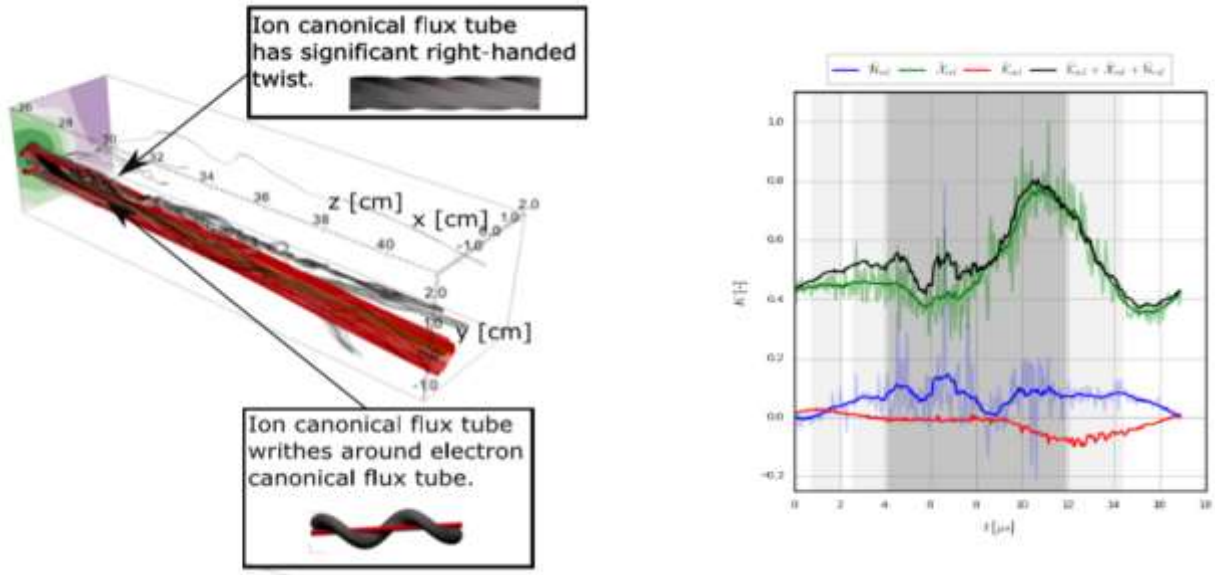

Figure 3. Techniques developed by the Mochi project used to reconstruct (left panel) canonical flux tubes in the RSX experiment; canonical flux tubes are tubes of constant canonical vorticity, the circulation of a species canoical momentum $\boldsymbol{P} = nm\boldsymbol{u} + nm\boldsymbol{A}$; the techniques used massive datasets of 3D magnetic probes, Mach probes, and triple probes to obtain each species density *n*, each species flows $\boldsymbol{u}$ and magnetic vector potential $\boldsymbol{A}$; the ion canonical flux tube (black) launches from the same footpoints as the electron (red) flux tube. The electron flux tubes are topologically equivalent to magnetic flux tubes. These first visualizations of real ion canonical flux tubes show that they writhe around magnetic flux tubes. The same techniques calculate the evolution of three types of helicities (right panel): flow helicity in blue, cross-helicity in green and magnetic helicity in red. Cross-helicity dominates in RSX.

for >40 Alfvén times despite the plasma parameters being in classically-unstable space (Fig. 2). The apparatus is unique because it has three nested electrodes to mimic the azimuthal shear rotation profile of an accretion disk, and azimuthally symmetric gas slits so the location of mass sources does not hinder

	Particle regime	Kinetic regime	Fluid regime
Canonical momentum $\vec{P}_\sigma$	Definition: $\vec{P}_\sigma^{par} \equiv \gamma m_\sigma \vec{v}_\sigma + q_\sigma \vec{A}$ Newtonian limit: $\vec{P}_\sigma^{par} = m_\sigma \vec{v}_\sigma + q_\sigma \vec{A}$	Definition: $\vec{P}_\sigma^{kin} \equiv f_\sigma \vec{P}^{par}$ Newtonian limit: $\vec{P}_\sigma^{kin} = f_\sigma m_\sigma \vec{v}_\sigma + f_\sigma q_\sigma \vec{A}$	Definition: $\vec{P}_\sigma^{flu} \equiv \int \vec{P}_\sigma^{kin}\, d\vec{v}_\sigma$ Newtonian limit: $\vec{P}_\sigma^{flu} = \rho_\sigma \vec{u}_\sigma + \rho_{c\sigma}\vec{A}$
Enthalpy h_σ	Definition: $h_\sigma^{par} \equiv \gamma m_\sigma c^2 + q_\sigma \phi$ Newtonian limit: $h_\sigma^{par} = \frac{m_\sigma v_\sigma^2}{2} + q_\sigma \phi$	Definition: $h_\sigma^{kin} \equiv f_\sigma h_\sigma^{par}$ Newtonian limit: $h_\sigma^{kin} = f_\sigma \frac{m_\sigma v_\sigma^2}{2} + f_\sigma q_\sigma \phi$	Definition: $h_\sigma^{flu} \equiv \int h_\sigma^{kin}\, d\vec{v}_\sigma$ Newtonian limit: $h_\sigma^{flu} = \rho_{c\sigma}\phi + \frac{1}{2}\rho_\sigma u_\sigma^2 + \mathcal{P}_\sigma$
Canonical vorticity $\vec{\Omega}_\sigma \equiv \nabla \times \vec{P}_\sigma$	Newtonian limit: $\vec{\Omega}_\sigma^{par} = m_\sigma \vec{\omega}_\sigma^{par} + q_\sigma \vec{B}$ where $\vec{\omega}_\sigma^{par} = \nabla \times \vec{v}_\sigma$	Newtonian limit: $\vec{\Omega}_\sigma^{kin} = f_\sigma \vec{\Omega}_\sigma^{par} + \nabla f_\sigma \times \vec{P}_\sigma^{par}$	Newtonian limit: $\vec{\Omega}_\sigma^{flu} = \rho_\sigma \vec{\omega}_\sigma^{flu} + \rho_{c\sigma}\vec{B} + \nabla n_\sigma \times (m_\sigma \vec{u}_\sigma + q_\sigma \vec{A})$ where $\vec{\omega}_\sigma^{flu} = \nabla \times \vec{u}_\sigma$
Canonical force-field $\vec{\Sigma}_\sigma \equiv -\nabla h_\sigma - \frac{\partial \vec{P}_\sigma}{\partial t}$	Newtonian limit: $\vec{\Sigma}_\sigma^{par} = q_\sigma \vec{E} - \nabla\left(\frac{m_\sigma v_\sigma^2}{2}\right) - m_\sigma \frac{\partial \vec{v}_\sigma}{\partial t}$	Newtonian limit: $\vec{\Sigma}_\sigma^{kin} = f_\sigma \vec{\Sigma}_\sigma^{par} - h_\sigma^{par} \nabla f_\sigma - \vec{P}_\sigma^{par} \frac{\partial f_\sigma}{\partial t}$	Newtonian limit: $\vec{\Sigma}_\sigma^{flu} = \rho_{c\sigma}\vec{E} - \nabla\left(\frac{\rho_\sigma u_\sigma^2}{2} + \mathcal{P}_\sigma\right) - \frac{\partial(\rho_\sigma \vec{u}_\sigma)}{\partial t}$

Table 1. Definitions of the canonical momentum and enthalpy of the species σ with the resulting canonical fields. The species particles have mass m_σ, charge q_σ, a velocity distribution function $f_\sigma(\vec{v}_\sigma)$, which could be integrated as usual to the fluid regime with mass density ρ_σ, the charge density $\rho_{c\sigma}$, flowing at the bulk velocity $\vec{u}_\sigma$ with pressure $\mathcal{P}_\sigma$. (see Ref. [Product 6.1.3] for details) The electromagnetic field is defined by the electrostatic potential ϕ and magnetic potential $\vec{A}$. The symbols $\gamma(\vec{v}_\sigma)$ and c represent the Lorentz factor and the speed of light, respectively.

Definition of gauge-invariant canonical helicity	$K_\sigma \equiv \int \vec{P}_{\sigma-} \cdot \vec{\Omega}_{\sigma+}\, dV$
Equation of motion (all regimes)	$\vec{\Sigma}_\sigma + \vec{v}_\sigma \times \vec{\Omega}_\sigma = \vec{R}_\sigma$
Canonical helicity evolution equation	$\frac{dK_\sigma}{dt} = 2\int (\vec{R}_\sigma \cdot \vec{\Omega}_\sigma)_-\, dV + \int h_{\sigma-}\, \vec{\Omega}_\sigma \cdot d\vec{S} + \int \vec{P}_{\sigma-} \times \frac{\partial \vec{P}_{\sigma+}}{\partial t} \cdot d\vec{S} + \int \vec{P}_{\sigma-} \cdot \vec{\Omega}_{\sigma+}\, \vec{u}_\sigma \cdot d\vec{S}$

Table 2. Overview of canonical helicity transport equations (see Ref. [Product 6.1.3] for details). Helicity is defined using the canonical momentum defined in Table 1 for the chosen regime. The + and – subscripts include reference fields to make helicity gauge invariant. The equation of motion in this Ohmic form is the same for all regimes, and can be derived from a Lagrangian-Hamiltonian point-of-view (see Fig. 9 for an overview and Ref. [Product 6.1.3] for details), to give the usual forms of the equations of motion (single particle, Vlasov eqution, multi-fluids, and MHD). This form of the equation of motion then gives the canonical helicity evolution equation (row 3) which is valid in all regimes. Dissipative forces are represented by $\vec{R}_\sigma$ and any motion of the system boundary is $\vec{u}_\sigma$.

rotation. Measurements show that the jet is stable when there are helical shear flows and is unstable in the absence of azimuthal shear flows, as hypothesized. This accomplishment succesfully addresses objectives defined in Section 3 of the Project Narrative (elements 3.1 to 3.4), some research objectives (elements 4.1, 4.2, 4.4), the main scientific goal, and scientific question a.

The time evolution of magnetic helicity has not yet been measured in the Mochi experiment because the magnetic probes were completed only just before early-termination of the project. But the project developed the techniques necessary for calculating the time evolution of all forms of helicity (magnetic, cross, flow, and canonical) from massive datasets of magnetic and flow measurements (~3000 repeated shots with 3D time-resolved Bdot probes, triple and Mach probes). While waiting for the Mochi experiment to become operational, the techniques were applied on existing datasets from the retired Reconnection Scaling Experiment (RSX). The results (Fig. 3) are the first to present the time evolution of all forms of helicity in an experiment, and show that cross-helicity dominates other forms of helicity in RSX's rotating, kinked magnetic flux ropes. The data is inconclusive on conversion of magnetic helicity to helical flows (scientific question b) probably because the RSX data was obtained only for a single flux rope that did not evolve or reconnect. The work also presented the first 3D visualization of canonical helicity in an experiment (Fig. 3, scientific questions b and d).

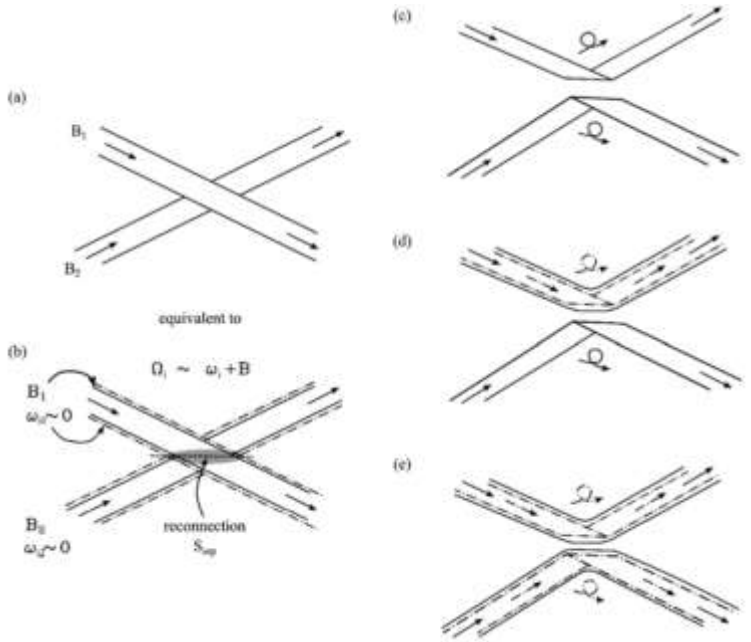

Figure 4. Merging of canonical flux ropes (reduced two-fluid regime). (a) Magnetic flux ropes with one crossing, giving a total initial magnetic helicity of 1 unit. This is equivalent to (b) two crossing canonical flux ropes with no flow vorticity. Merging reconnection occurs at a separation surface S_{sep} with a non-uniform enthalpy into equation (Table 2, row 3) that can result in one of three scenarios: (c) two canonical flux ropes with no flow but a half-twist magnetic flux, i.e. two magnetic flux ropes, conserving total canonical helicity and magnetic helicity;(d) two canonical flux ropes, one with a half-twist flow vorticity but no magnetic twist and the other with a half-twist magnetic flux but no flow twist, after converting part of the magnetic helicity in the initial crossing into flow twist, conserving total canonical helicity;(e) two canonical flux ropes, each with a half-twist flow vorticity and no magnetic twist, still conserving total canonical helicity..

4.3. Theoretical accomplishments

The project has successfully developed a two-fluid helicity transport model for flux-rope merging (scientific questions b, c, d; research objectives 4.1, 4.2, Ref. [Product 6.1.4]). The model provides the conditions for when the transport of canonical helicity during merging manifests itself as magnetic helicity transfer or as generation of strong helical plasma flows (Fig. 4). Canonical helicity is defined as the gauge-invariant helicity of the canonical momentum a given species (see Tables 1 & 2, and Refs. [Products 6.1.2, 6.1.3] for mathematical definitions). The model is succesfully applied to explain the bifurcation in compact torus merging observed on the TS-4 experiment (scientific question c, research objective 4.2). The model is also relevant to situations where magnetic flux-ropes and flow vorticity flux-ropes interact, such as in astrophysical jets or magnetic nozzles. The model shows that the topological property of interest, canonical helicity, can be transferred from one fluid to another fluid while preserving the total canonical helicity. With the appropriate inductive or enthalpy boundary conditions, magnetic field line pitch in flux rope can decrease to increase helical plasma flows or, conversely, flow line pitch could decrease to increase the helicity of magnetic field lines (research objective 4.1).

The project has theoretically explored the possibility of sausage instabilities developing on top of a kink instability in lengthening current-carrying magnetic flux tubes (Fig. 5, research objective 4.3, Ref. [Product 6.1.1]). Observations indicate that the dynamics of magnetic flux tubes in our cosmos and terrestrial experiments can involve topological changes faster than time scales predicted by resistive magnetohydrodynamics. Recent laboratory experiments suggest that hierarchies of instabilities, such as kink and Rayleigh-Taylor, could be responsible for initiating fast topological changes by locally accessing two-fluid and kinetic regimes. Sausage instabilities can also provide this coupling mechanism between disparate

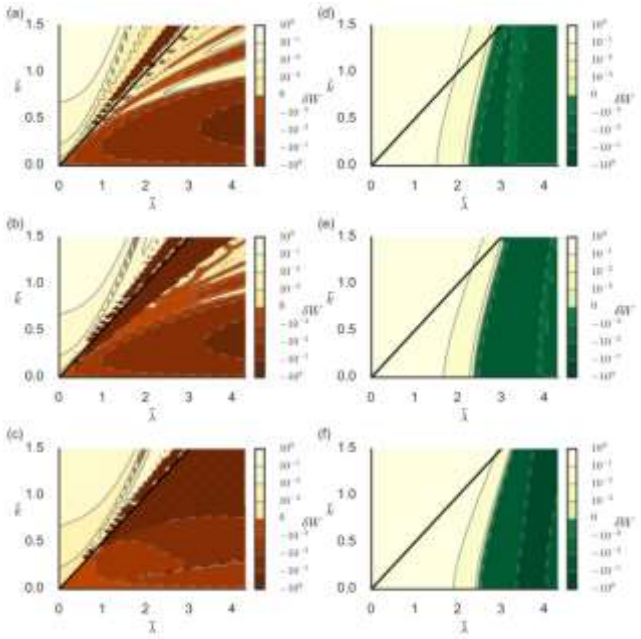

Figure 5. Numerical $k - \lambda$ stability spaces with relative growth rates (contours) for kink instabilities (left column) and sausage instabilities (right column). The straight black line is the classical Kruskal-Shafranov threshold. The rows correspond to the same parameters $\epsilon_{eff} = 0.7, 0.5, 0.1$, respectively. The parameter represents the hollowness of the current-profile in the magnetic flux tube. The cross-hatched regions are the Suydam unstable regions. This stability space can be compared to Fig. 2d.

scales (Ref. [Product 6.1.1]). Flux tube experiments can be classified by the flux tube's evolution in a configuration space described by a normalized inverse aspect-ratio k and current-to-magnetic flux ratio λ (Fig. 5). A lengthening current-carrying magnetic flux tube traverses this k–λ space and crosses stability boundaries. We have derived a single general criterion for the onset of the sausage and kink instabilities in idealized magnetic flux tubes with core and skin currents. The criterion indicates a dependence of the stability boundaries on current profiles and shows overlapping kink and sausage unstable regions in the k–λ space with two free parameters. Numerical investigation of the stability criterion reduces the number of free parameters to a single parameter that describes the current profile and confirms the overlapping sausage and kink unstable regions in k–λ space. A lengthening, ideal current-carrying magnetic flux tube can therefore become sausage unstable after it becomes kink unstable. The plasma jets in the Mochi experiment are succesfully tracked inside this stability space, crossing into the kink unstable region but have yet to reach the sausage unstable region (Fig. 2d, research objective 4.4).

The project has published a detailed analytical examination of the morphology of astrophysical jets from a canonical flux tube point-of-view (scientific questions a, b, d; research objectives 4.1, 4.2; Ref. [Product 6.1.2]). Magnetized plasma jets are generally modeled as magnetic flux tubes filled with flowing plasma governed by magnetohydrodynamics (MHD). The project outlines a more fundamental approach based on flux tubes of canonical vorticity, where canonical vorticity is defined as the circulation of the species' canonical momentum. This approach extends the concept of magnetic flux tube evolution to include the effects of finite particle momentum and enables visualization of the topology of plasma jets in regimes beyond MHD. A flared, current-carrying magnetic flux tube in an ion-electron plasma with finite ion momentum is thus equivalent to either a pair of electron and ion flow flux tubes, a pair of electron and ion canonical momentum flux tubes, or a pair of electron and ion canonical vorticity flux tubes. The morphology of all these flux tubes are examined for increasing electrical currents, different radial current profiles, different electron Mach numbers, and a fixed, flared, axisymmetric magnetic geometry. Calculations of

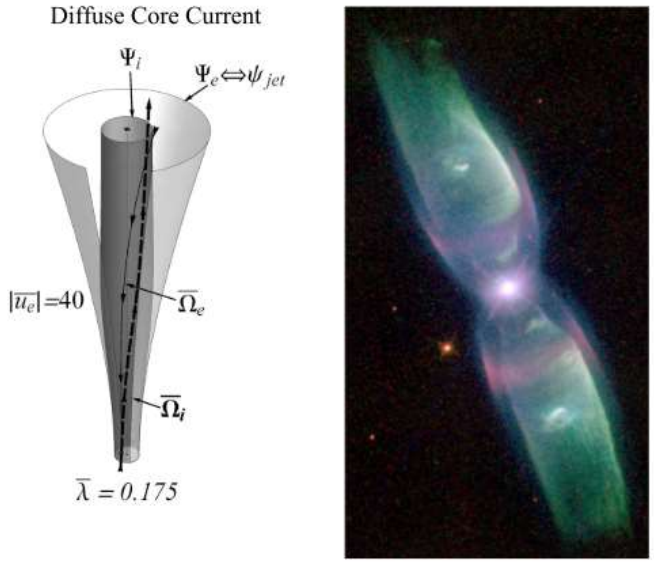

Figure 6. (Left) Bulged ion canonical vorticity flux tube $\Psi_i = \int \boldsymbol{\Omega}_i \cdot d\boldsymbol{S}$ (dark gray) for a diffuse core current jet with low current (λ = 0.175) and a large electron velocity (| u_e | = 40). Equation (row 2 Table 2) shows that density gradients can be normal to the dark gray canonical Ψi surfaces rather than the light gray magnetic flux surfaces ψ suggesting that ion line emission reveals canonical flux tubes as opposed to magnetic flux tubes. (Right) M2-9 Butterfly nebula (NASA HSTSTIS/CCD—MIRVIS), a bipolar planetary nebula with distinctive bulging that resembles the ion canonical flux tube in the left panel. Transitions in the geometry of the jet (i.e., flaring to collimation) may therefore also reflect changes in the relative strength of the fluid flow vorticity flux to the magnetic flux. Image credit: Bruce Balick (University of Washington), Vincent Icke (Leiden University), Garret Mellema (Stockholm University), and NASA.

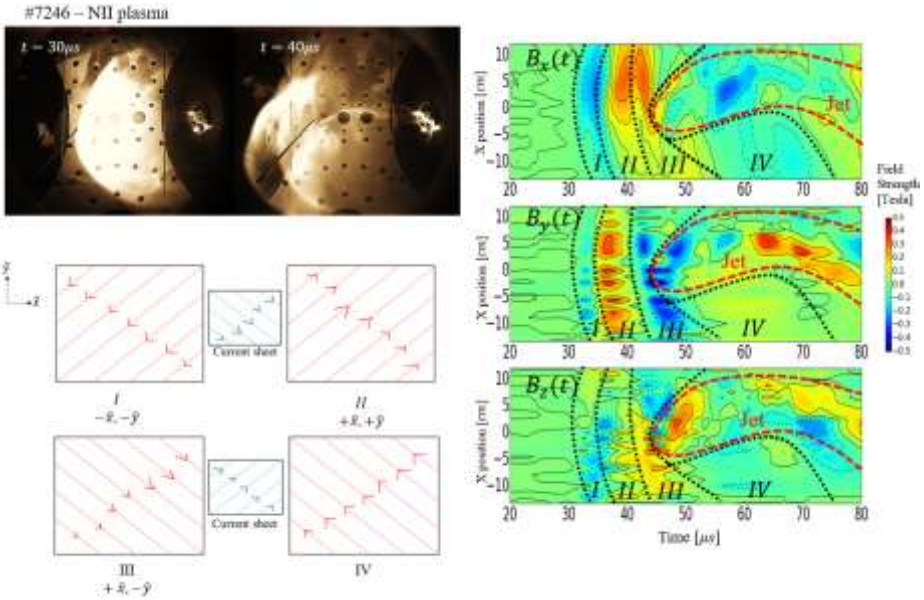

Figure 7. Two bow-shocks observed in the Mochi.LabJet experiment. The magnetic probes measure two current sheets, one between time periods I and II, and a second between time periods III and IV. The orientation of the magnetic field flip as the current sheets travel past the probes (bottom left panels). The second magnetic bow shock appears to be deformed by the long plasma jet impacting from behind.

gauge-invariant relative canonical helicities track the evolution of magnetic, cross, and kinetic helicities in the system, and show that ion flow fields can unwind to compensate for an increasing magnetic twist. The results demonstrate that including a species' finite momentum can result in a very long collimated canonical vorticity flux tube even if the magnetic flux tube is flared. With finite momentum, particle density gradients

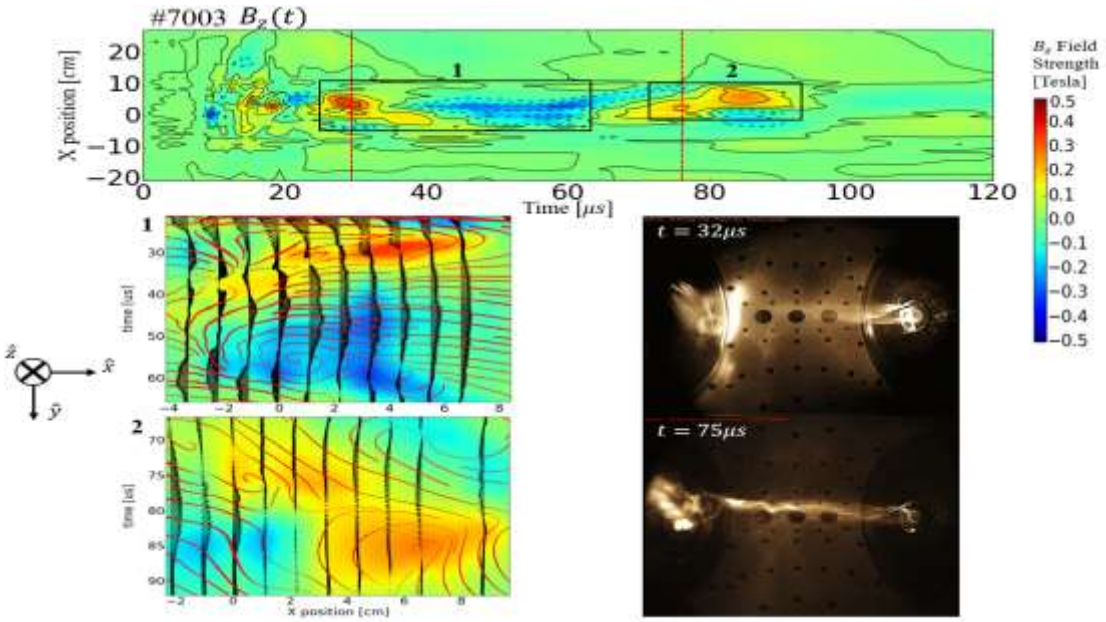

Figure 8. Double-helix magnetic configuration observed in the Mochi.LabJet experiment. As the plasma jet blows by the magnetic probe array (bottom right), the probes measure a pair of helical magnetic flux tubes (upper panel) with opposite axial magnetic fields and current densities (cross-sections on bottom left panels). The magnetic structure appears to be consistent with an elongated Taylor state.

must be normal to canonical vorticities, not to magnetic fields, so observations of collimated astrophysical jets could be images of canonical vorticity flux tubes instead of magnetic flux tubes (Fig. 6).

4.4. Unexpected interesting results

4.4.1. Double-helix relaxed state in Mochi.LabJet

In Mochi.LabJet, analysis of the existing magnetic measurements demonstrates the existence of two bow shocks (Fig. 7) and a relaxed magnetic configuration resembling a double-helix elongated Taylor state (Fig. 8). This was not predicted. These laboratory results resemble observations of double-helix structures in real astrophysical jets (e.g. double helix nebula). The double-helix state is a cousin of the elongated Taylor states first observed in the Swarthmore Spheromak Experiment (SSX). Unlike in SSX, the Mochi states were produced without an elongated solid material flux conserver. In the case of Mochi, detailed observations of the formation sequence suggest that there is a plasma flux conserver. The plasma flux conserver formed from the remnants of an initial plasma jet that detached from the source gun to travel while decelerating into the surrounding vacuum and looking like an umbrella-shaped plasma (first bow shock). Driven by the remaining power in the gun, a second plasma jet forms and shoots into the umbrella (second bow shock). The working hypothesis is that the umbrella acts as a flux conserver because a plasma has good conductivity and the second jet can therefore relax to an elongated double-helix Taylor state. A manuscript is in preparation (Ref. [Product 6.2.5]).

4.4.2. Canonical field theory

The project developed a field theoretical approach to the evolution of canonical helicity (Fig. 9). The field theory is necessary to fully generalize the concepts of plasma self-organization to realistic regimes, for example kinetic regimes, relativistic regimes, or configurations with density gradients. Self-organization is concerned with the spontaneous emergence of large-scale structures in physical systems. A fundamental

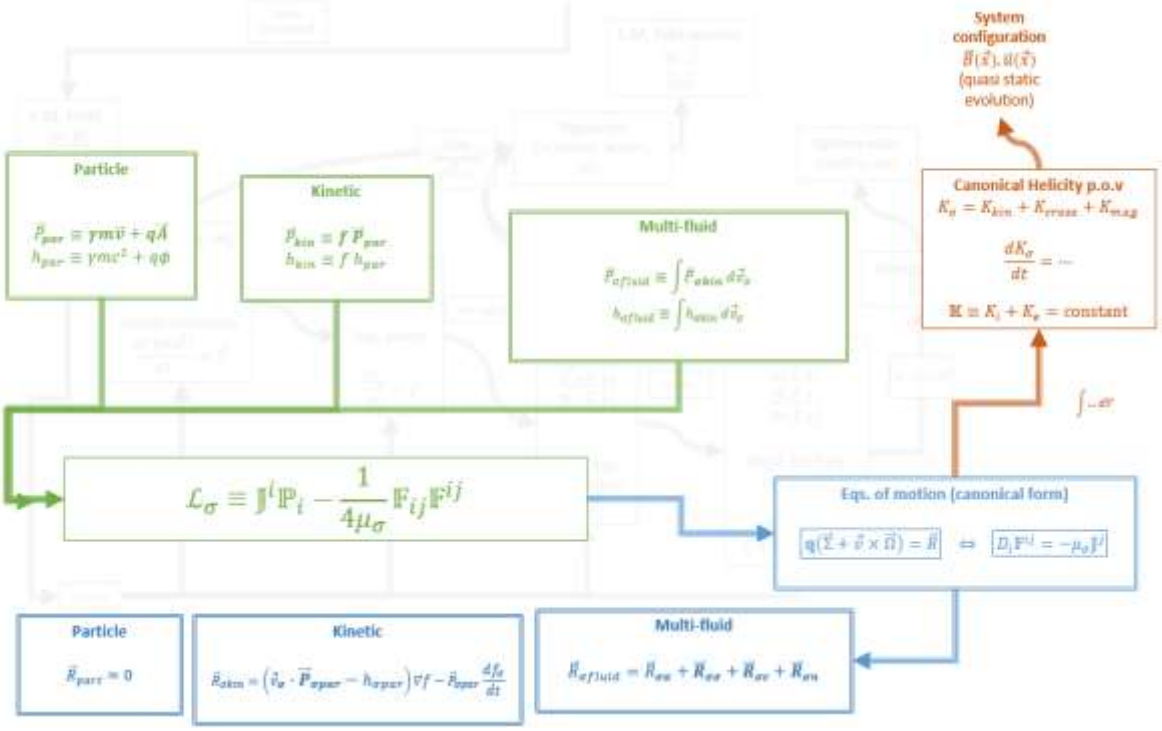

Figure 9. Overview of canonical field theory (see Ref. [Product 6.1.3] for details). The starting point (green) are definitions of the canonical momentum and enthalpy in a given regime (Table 1). These field quantities form the Lagrangian $\mathcal{L}_\sigma$ of the species, expressed here in tensor form suitable for general relativistic regimes. The Lagrangian results in the equations of motion (blue) that can be written as an Ohm's law (equation of row 3, Table 2) or equivalently in Maxwell's equations form. The equation of motion in Ohm's law form then results in the helicity transport equations (red, row 4 of Table 2) that can be used to determine the system configuration. The ususal magnetostatic or hydrodynamic formulations are retrieved with $m \to 0$ and $q \to 0$, respectively.

conjecture, borrowed from the mathematics of topology, is the invariance of a global property during the process of self-organization: for example, a system relaxes to reduce energy but is constrained by a constant value of the helicity of a vector field. Above a critical threshold, the system then forms a large-scale structure of that specific vector field. Hydrodynamic flow helicity models have been applied to the forecasting of tornadoes, knotting of DNA, entanglement of polymers, and wing-tip vortices. Magnetic field helicity models are the foundation of theories for the origin of cosmic magnetic fields, astrophysical jets, solar coronal loops, and toroidal magnetic confinement concepts. Arguments ranging from maximal entropy to selective decay attempt to justify why helicity is conserved while energy is minimized, leading to magnetic-, neutral-, or at best, multi-fluid relaxation models. Earlier work has demonstrated an isomorphism between two-fluid plasmas and Maxwell's equations and investigated the helicity of a fluid in a relativistic context. But a severe limitation is that all these theories rest on simple and restrictive descriptions of fluids and plasmas: Euler equations for fluids, magnetohydrodynamic or barotropic multi-fluid equations for plasmas. The field theory developed by the project shows that the fundamental transport equation governing helicity evolution is valid across all classical field theory, including relativistic, single particle, kinetic, and fluid regimes. The framework takes into account dissipation, collisionless situations, collective behavior, particle reactions, and electromagnetic interactions. This new formulation is derived directly in a Lagrangian-Hamiltonian framework and results in a canonical form of the equation of motion expressed as an Ohm's law or, equivalently, as Maxwell's equations for canonical fields.

This field theory approach shows that in a simple dissipative system, if the density gradient is weak, helicity changes more slowly than total energy, but if the density gradient is large, helicity changes more rapidly than total energy. This is a first principles explanation for the ruggedness of helicity invariants with

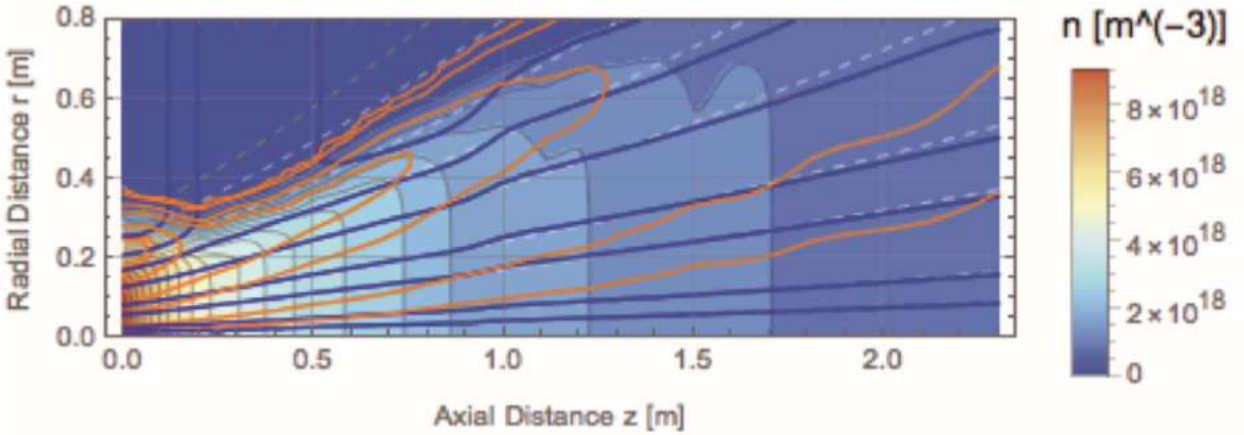

Figure 10. Comparison of canonical field theory calculations of ion flux surfaces (blue lines), ion canonical vorticity flux surfaces (orange lines), ion number density (contours) from published VASIMR data (details in Ref. [Products 6.4.2]. The magnetic flux surfaces are dashed blue and the mathematical edge of the plume is dashed yellow. The calculated ion flux surfaces lie on the magnetic flux surfaces, except towards the the plume edges (or far downstream z>1.7m). This contradicts the published conclusion by the VASIMR group that ion flux surfaces separate earlier from magnetic flux surfaces. Their claim is based on ion flux inferred from Langmuir probe measurements not from ion flow measurements from Mach probes. Our theory predicts a return ion flow at the plume edges, since ions follow the canonical vorticity flux surfaces (orange). This also explains the divergence of the caclulated ion flux lines at the throat (0.2<z<0.5m): the calculations folow the VASIMR calculation of ion flux inferred from Langmuir probes directed in the negative z direction and could therefore not measure the return flow. A manuscript is in preparation.

respect to energy conservation and provides a criterion for determining where and when constrained relaxation is applicable.

This field theory approach to helicity and energy evolution suggests that techniques borrowed from electromagnetism would be suitable for analyzing self-organization and magnetic reconnection, similar to how existing analysis of helicity injection into toroidal magnetic configurations uses electrical circuit analysis techniques. For example, electrical circuit methods were used to analyze the constrained relaxation of driven magnetostatic configurations (Eq. of row 3 Table 2 with $m \to 0$). Concepts of alternating or direct currents, voltages, impedances, resonances, etc., were useful and practical because a magnetostatic plasma is an electrical load for the driving circuits. The Maxwell form of the unifying Lagrangian confirms that electrical engineering methods are useful for magnetostatic plasmas and suggests that such methods should also be useful for flowing magnetized (or non-magnetized) plasmas and flowing neutral fluids with finite vorticity. The driving circuits can be any combination of gravitational, pressure, kinetic, or electrical supplies since these power supplies are simply enthalpy sources for a canonical Maxwell circuit. On the largest scale, adding Einstein's Lagrangian to the canonical field theory Lagrangian would extend the concept of self-organization by helicity-constrained relaxation to general relativity. This has applications, amongst others, to astrophysical jet formation from accretion disks around super-massive black holes in active galactic nuclei, or the cosmological early Universe.

4.4.3. Magnetic nozzles

An astrophysical jet can be thought of as a natural magnetic nozzle. The mechanism for plasma detachment has been investigated with canonical field theory, and compared to recent reported observations of plasma detachment in a plasma thruster by the Variable Specific Impulse Magnetoplasma Rocket (VASIMR) group (Fig. 10). Canonical field theory is a recent unifying framework for kinetic and fluid models capable of considering non-ideal physics with a generalized Maxwell formulation. Analytical fits to the published experimental data shows that constant ion flux surfaces do not separate from constant magnetic flux surfaces, in contradiction with the reported observations. The difference comes from a subtle error by the VASIMR group in defining the ion flux surface quantity in the published result. Our theoretical analysis is however consistent with the other two key indicators of plasma detachment observed in the reported experiment. Our

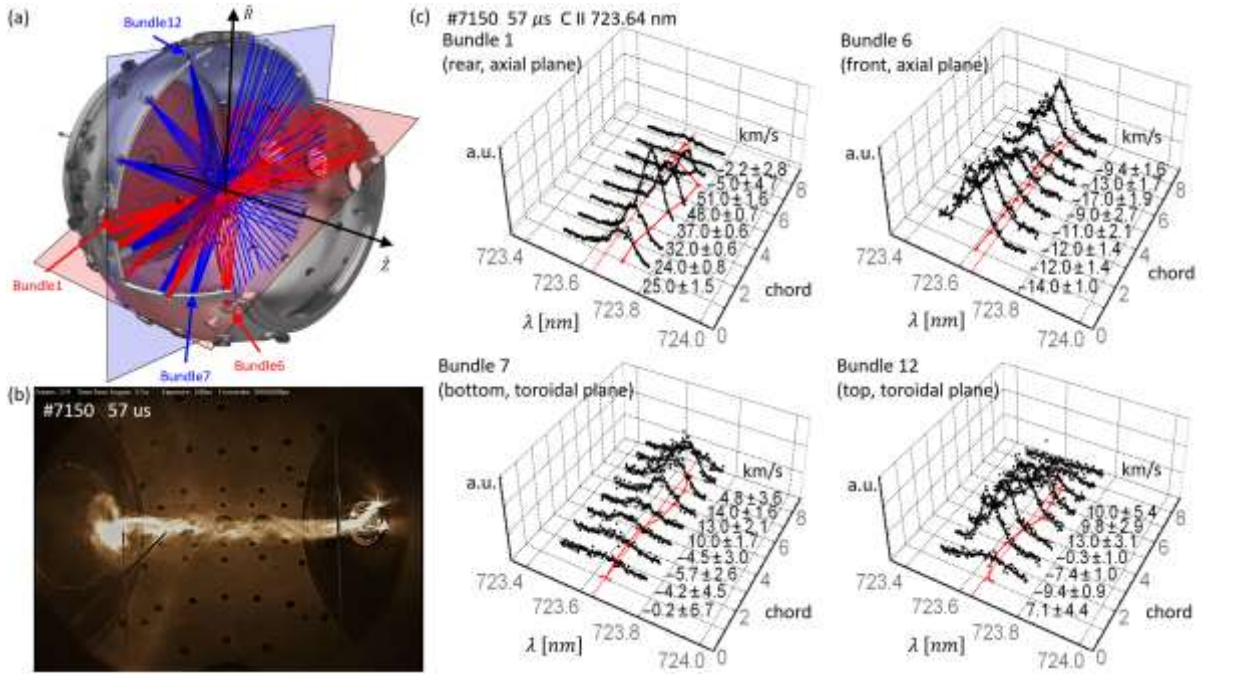

Figure 11. Multichannel optical spectroscopy on the Mochi experiment: (a) 96 viewchords arranged in two planes, bundles number 1 to 6 with 8 view chords each in the poloidal axial plane (red), and bundles number 7 to 12 with 8 view chords each in the toroidal plane (blue); (b) fast imaging frame of a stable collimated plasma jet from discharge #7150 at 57 μs, for which (c) the C II 723.642nm line measurements show a distinct red shift for bundle 1 and a blue shift for bundle 6 indicating axial plasma flows, and bundles 7 and 12 measure blue and red shifts consistent with azimuthal rotation.

theory suggests the plasma is attached to magnetic flux surfaces near the axis and throat exit. Around the plume edge region, the plasma separates from the magnetic flux surfaces but is tied to canonical vorticity flux surfaces. The analysis predicts a returning plasma flow at the edge plasma. This returning plasma flow has not been measured by the VASIMR group because they used triple electrostatic probes facing the thruster to infer plasma flows instead of using Mach probes. A manuscript is in preparation with details in Ref. [Products 6.4.2].

4.5. Objectives not completed or made obsolete considering new results

The objective element 3.5, perform vector tomographic reconstruction of ion Doppler spectroscopy, is incomplete. The element consists of two parts: writing the computer software and building the multi-chord spectroscopy diagnostic (related to objective element 3.4.2, see next paragraph). The algorithm has been optimized to improve reconstruction by a factor of more than 10 in speed by re-writing the code in C instead of the original IDL. A separate code has been written to facilitate conversion of experimental line-of-sight coordinates into the mathematical coordinates necessary for reconstruction. To quantify uncertainty in reconstruction, the project implemented two methods for comparing vector fields: one based on histograms of vector field properties (root mean square of magnitude and orientation), and another based on a Taylor diagram of three vector field properties (a similarity coefficient, a root mean square difference, and a root mean square length). The similarity coefficient can be understood as a normalized helicity density sum between two vector fields. This second method is the technique developed for analyzing the canonical helicity reconstructions from the RSX data (Section 1.1). The complete software is operational, although made of these disparate parts, still await complete integration into a single user-friendly package.

The multi-chord optical spectroscopy (objective element 3.4.2) was completed in April 2017 for 96 chords (Fig. 11). The diagnostic consists of a dual frame iCCD camera mounted on a 1 m focal length monochromator with 2400 l/mm grating, coupled to a custom fiber-optic bundle with 96 optical fibers grouped into 12 bundles of eight 100 um cores at the plasma side, and three vertical lines at the monochromator side. The fiber-bundle was constructed in-house at a record cost of ~$27/chord. The cost savings were significant mainly due to 3D printing of parts using a commercial consumer-level printer available in-house. The number of chords is sufficient to observe shear helical flows in the plasma jet (Fig. 11) from Abel inversion or simple fits (manuscript in preparation, Ref. [Products 6.2.2]). But the number remains insufficient to observe the complete 3D flow structure in the plasma jet from computer vector tomography. More time, a few more cameras and monochromators, and extra fiber-bundles were planned to increase the number of chords to 512 to cover all 64 viewports of the spherical vacuum chamber, and capable of providing sufficient data for vector tomographic reconstruction.

The proposed research element 4.1 is incomplete, and is possibly obsolete considering the new results of Sections 4.2 and 4.4. The plasma jet produced by the Mochi experiment is stable as hoped. But it appears stable not due to $q < 1$ as magnetic helicity is converted to flow helicity, but because of helical shear flows even if $q > 1$. Furthermore, the elongated double-helix relaxed state makes it non-trivial to determine the classical safety factor. This does not preclude the possibility of conversion of magnetic helicity into flow helicity, but this line of investigation requires further effort: direct measurements of the evolution of the safety factor and the flow profiles. Given more time, this effort would be possible on the existing apparatus.

The proposed research element 4.2 is incomplete due to early termination of the project. However, preliminary plasma shots with higher Z gas (Ar and N) were performed (Fig. 7). Using different gas species allows independent experimental control of the size parameter S* (ratio of Larmor radius to plasma scale length). The plan was to scan canonical helicity injection into the plasma jet at various S* and see if helicity is preferentially channeled into flows or into magnetic fields, as predicted by the canonical field theory. The higher Z gas shots showed stronger deformation of the bow shocks by the secondary jet, but quantitative flow measurements were not complete enough to provide any definitive conclusion yet.

5. Summary of project activities for the entire period of funding

The following summary of project activities are extracts of the yearly progress reports.

5.1. Year 1 (Jul 2013 – Apr 2014)

Vacuum chamber. The design has been finalized, the vendor's drawing has been approved and the item has been released to manufacture with an estimated delivery date of mid-June 2014. The final cost is $95k. The $35k amount over budget is offset by the cheaper-than-anticipated cryopump purchase, and may be compensated further by other equipment items which are potentially below budget (plasma gun, digitizers). MDC heavily discounted their quote to match Lesker. The final quotes from other vendors were $95k (Lesker), $130k (Norcal), $200k (Spincraft), $300k (Atlas UHV), $750k (Portage Casting and Mold). The spherical design and the large number of ports/viewports (over a hundred) resulted in manufacturing costs that exceeded projections. The chamber is unique in providing 72 viewports arranged spherically around a plasma volume dedicated to vector tomography of ion spectroscopy. This will allow reconstruction of plasma density and plasma flows in 3D.

Cryopump and compressor. The item has been ordered from SHI Cryogenics with an estimated delivery in May 2014. The final cost was $18k, which is $12k below budget. The final cost included a University discount that was not anticipated.

Plasma gun assembly. The design is still being finalized but sufficiently developed to begin purchasing several off-the-shelf parts ($5.8k to date, vacuum tubing and ceramic breaks). The copper material for the electrodes are being quoted. The design iterations aims to achieve a final cost about $14k lower than the budgeted amount (35% lower) thanks to a simplification in the design and most of the machining done in-house instead of being outsourced. The remaining balance should help offset the vacuum chamber final cost. The estimated completion date is on schedule for July 2014.

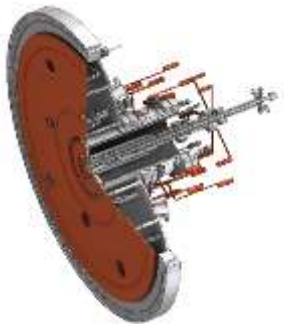

Digitizers and data acquisition. The software for acquiring and saving data is nearly complete. Data is stored in MDSplus for standardization with other plasma research laboratories. The process for selecting new digitizer modules is ongoing, with the goal of achieving a final cost $10k below the budgeted $30k to offset the vacuum chamber cost, but without reducing the number of digitizing channels. Most of the channels are for magnetic probes.

HV capacitor banks. Two out of four capacitor banks have been completed, with the assembly of the next two underway. The estimated completion date is on schedule for July 2014 ("first plasma" expected). For safety, all the banks are remotely and optically controlled (triggers, voltage settings, voltage and current readouts). The two completed banks have been successfully tested on the test chamber and test plasma gun (successful magnetized plasma discharges).

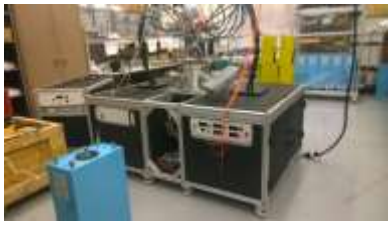

Experimental control. The hardware and software for controlling the experiment has recently been completed and is now operational. The control system remotely operates all the capacitor banks to improve

operational safety and to protect low-voltage equipment. The control system is also designed to operate all other electrical equipment (gas valves, gate valves, pumps, diagnostics, etc.).

Diagnostics.

- Magnetic probes: on schedule for completion by September 2014.
- Tomography spectroscopy: fiber mounts and translation platforms have been purchased ($1.8k) ahead of Year 2 to provide values of spectral resolution and spatial resolvability of the monochromator setup to inform the final design of the fiber-bundle. The design should be finalized by July 2014 in anticipation of Year 2 of the project. The tomographic reconstruction software is being optimized for shot-to-shot reconstruction with all the lower-level routines converted into C++ for high-speed calculations.
- Other diagnostics: Rogowski coils, and high voltage probes have been successfully completed and tested/calibrated on the small test chamber. An interferometer is currently being built.

Scientific progress and dissemination. The project's progress and theory behind the project has been presented at several conferences (APS DPP 2013 in Denver, CO; invited talk at EPR 2013 in Fort Worth, TX; invited talk at IPELS 2013 in Hakuba, Japan). Theoretical work found that magnetic flux tubes can reconnect with tubes of helical flow (vorticity) in such a way as to conserve a total amount of (generalized) helicity. This hints at a conservation rule more powerful than magnetic helicity conservation. An invited paper which develops the mathematical details and proposes an intuitive picture of reconnection between generalized flux tubes has recently been published [S. You, "A two-fluid helicity transport model for flux rope merging", *Plasma Phys. Control. Fusion*, **56**, 064007 (2014), doi:10.1088/0741-3335/56/6/064007]. The work has also been presented as invited seminars at Washington State Univ. (Pullman, WA), Postech (Pohang, Korea), KAIST (Daejeon, Korea), Seoul National Univ. (Seoul, Korea). The stability of flux tubes with skin and core current profiles is being investigated with the DCON code for comparison with theory and anticipated experimental measurements. Theoretical work is progressing on developing the canonical helicity argument for astrophysical jet geometries.

5.2. Year 2 (Apr 2014 – Apr 2015)

Vacuum chamber. The vacuum chamber is operational after a 6 month delayed delivery (expected mid-June 2014, actual delivery mid-December 2014). The final total cost is $99 271, including $2k for a mating adapter to the pneumatic gate valve, and $2k for electropolishing. The cost of electropolishing was heavily subsidized by the manufacturer MDC as a courtesy for the delay in product delivery. Fig. 1 shows the vacuum chamber in its permanent position in the laboratory (room 013 of the AERB building at the University of Washington).

Cryopump and compressor. The cryopump was delivered May 2014. Mating to the pneumatic gate valve (donated by P. Bellan, Caltech) and mounting on the vacuum chamber was concluded December 2014 upon delivery of the vacuum chamber. The pump was successfully tested to 12 K and 10^{-6} torr on the vacuum

chamber with temporary cooling lines. The permanent chilled water cooling lines are being installed for estimated completion April 2015, when the cryopump will be fully operational.

LabJet Plasma gun assembly. The two (inner and middle) electrodes sub-assemblies are under manufacture. The design has been finalized, all raw materials (OFHC Cu, stainless steel) and most parts delivered. We are manufacturing in-house to save cost, except for electropolishing to be outsourced but some difficulties in machining stainless steel resulted in delays and some minor re-design work. The inner and middle electrodes should be completed by May 2015. The outer electrode design remains to be finalized and manufactured. The estimated date of completion is June/July 2015. First plasma is then expected shortly after.

HV capacitor banks. All four capacitor banks have been completed, tested and are now operational. One bank is connected to the MOCHI.Spheromak plasma gun assembly (renamed DRX plasma gun, on loan courtesy of S. C. Hsu, LANL). This assembly is mounted on the same vacuum chamber on the opposite end from the MOCHI.Labjet port. Breakdown and first plasma on this gun was obtained Feb 18, 2015 at 1:22 am. The three other capacitor banks will power the bias coil and the inner/outer electrodes of MOCHI.Labjet as soon as they are completed. The design and manufacture of the capacitor banks was done entirely in house by the PI and students. Our design for an opto-electronic tachometer charging circuit is currently pending a possible patent (U.S. provisional patent No. 62/072,269 filed October 29, 2014, UW Ref. No. 47101.01US1).

Digitizers and data acquisition. The software for acquiring and saving data is effectively complete. Data is stored in MDSplus for standardization with other plasma research laboratories. The decision on the exact digitizer model has been postponed to June/July 2015 to coincide with first plasmas. In the meantime, a request for evaluation units of high channel count FPGA-based digitizers has been made to National Instruments. Comparisons with other vendors (Struck Innovative System, Germany) for large number of channels (160 total) favours National Instruments ($200/channel compared to $700/channel). The lower bandwidth limits measurements to 30-100 ns time-scales at best, but is still capable of observing the evolution of global features at the expected Alfvén velocity time-scales. The setup will complement our exisiting PXI setup that has 24 channels at 2.5 MS/s.

Diagnostics.

- Magnetic probes: now scheduled for completion by July 2015. The probe array had to be redesigned to accommodate the numerous twisted-pair wires (from 138 inductor coils). The mounts on to the chamber are 3D printed in our laboratory.
- Tomography spectroscopy: The fiber-bundle design is still being finalized and has been pushed to the Summer 2015 (beginning of Year 3). The new estimated time-of-completion is due to the vacuum chamber delay, since the final port locations and setup informs the final design. Most of the effort of Year 2, particularly by graduate Research Assistant Evan Carroll, has been refocused on completing the plasma gun, power supplies and associated setup.
- Other diagnostics: Rogowski coils, and high voltage probes have been successfully completed and tested/calibrated. A He-Ne interferometer is near completion and a retarding grid energy analyzer is to be completed June 2015.

Scientific progress and dissemination. The project's progress and theory behind the project has been presented at the APS DPP 2014 in New Orleans, LA and the APS NW Section 2014 in Seattle, WA. The stability of flux tubes with skin and core current profiles is being investigated by a graduate Research Assistant, Jens von der Linden, with a custom numerical code for comparison with theory and anticipated experimental measurements. Jens von der Linden has successfully passed his General Exam and is expected

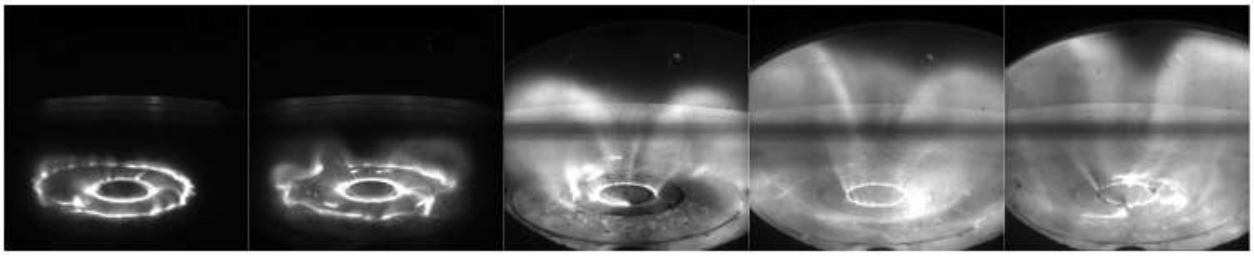

Fig. 12: Shot 3080 series (left to right time evolution 1-20 us approx.). The hydrogen plasma forms approximatel azimuthally symmetrically from the gas slits on the middle electrode to roughly the gas slits on the outer electrode (th inner electrode is not used here). The measured current between these two electrodes is ~13 kA for a gun voltage o 2.5 kV for a duration of ~60 μs (half-period) and bias magnetic flux of ~5 mWb at 0.3 T (estimated from bias coi current). The plasma begins to form a jet-like structure that expands out into the vacuum chamber.

Fig. 13: (left) Design of the Mochi.LabJet.Gun with azimuthally symmetric gas slits and three electrodes (inner, middle, and outer electrodes). (middle, right) Photographs of the gun mounted on the spherical vacuum chamber. The gas slits are designed to allow free rotation of the plasma jet. The three electrodes are designed to mimic rotation shear on accretion disks to form a core and skin plasma jets.

to defend before June 2016. Theoretical work is progressing on developing the canonical helicity argument for astrophysical jet geometries by a graduate Research Assistant E. Sander Lavine. A new theoretical framework for canonical momentum evolution is being developed by the PI that extends the existing canonical flux tube evolution theory to kinetic regimes. A manuscript is in preparation.

5.3. Year 3 (Apr 2015 – Apr 2016)

Experiment

First plasma. We achieved first plasma on Nov. 1, 2015 at 3am. The plasma was initiated between a pair of electrodes (the third innermost electrode was not powered) to test each component separately. We are currently testing all the components of the experiment step-by-step in our commissioning phase. The commissioning provides initial plasma jet configurations (Fig. 12) and uncovers issues in some of the hardware.

Vacuum chamber. The mating adapter to the pneumatic gate valve of the spherical chamber had a manufacturing default (large leak at the 14" rotating flange). MDC corrected the issue by sending a replacement without a rotating flange under warranty. In the meantime, the leak was sealed by Loctite 290, for a good base pressure of 3.3×10^{-7} torr.

Pumping system. The permanent chilled water cooling lines have been installed and completed during May 2015, when the cryopump became fully operational. As of today, the pump performs flawlessly. The $20k cost was borne by the Department. A 150 L/s small turbopump was mounted onto a 8" CF port (replacing the viewport) to help augment the cryopump, particularly for helium discharges. The backing dry scroll pump (Edwards XDS10) failed in February 2016. The quote for repair is ~$3k and remains to be decided.

LabJet Plasma gun assembly (Fig. 13). Completed Oct 2015 and mounted by the end of the month. The plasma gun is novel in its design with three concentric electrodes and azimuthally symmetric gas slits. The entire gun was designed and manufactured in-house, with major contribution by a very talented graduate student funded by this award (Evan Carroll). The design had tight tolerances in mounting three copper electrodes with stainless steel plenums for gas distribution. The plenums developed some leaks that were temporarily sealed with Torr-Seal high vacuum epoxy. The gas injection for the plasmas during our current commissioning phase (Fig. 1) used off-the-shelf Parker valves (S series) that did not perform as expected: the gas puff rise-time was about an order of magnitude too slow, so delivered too little gas at the slits compared to the gas in the rest of the chamber. These gas rise-time measurements were made with our custom-built fast-ion-gauge (2 μs response time, built by graduate student E. Sander Lavine). The fast ion-gauge is mounted on a moveable stalk inside the chamber to allow us to characterize the symmetry of the gas puff at plasma formation. These early plasmas and gas measurements showed that the Parker valves were not suitable for our purposes and I decided to make our own fast gas valves (based on the existing design from Paul Bellan of Caltech and Scott Hsu of LANL). The gas valves require another set of power supplies for triggering the gas valves. The design is finished and manufacturing is proceeding, with an expected completion by the end of April 2016. In total, the cost of the LabJet.Gun assembly, including the gas valves, gas power supplies, two electrode power supplies, bias coil power supply is ~37k. We expect to be back to plasma operations and commissioning of the rest of the equipment by early May 2016.

Digitizers and data acquisition (Fig. 14). The software for acquiring and saving data is effectively complete. Data is stored in MDSplus for standardization with other plasma research laboratories. High channel count FPGA-based digitizers has been purchased in June 2015 from National Instruments at $31k for 96 channels. Comparisons with other vendors (Struck Innovative System, Germany) for large number of channels (160 total) favours National Instruments ($350/channel compared to $700/channel). The lower bandwidth limits measurements to 30-100 ns time-scales at best, but is still capable of observing the evolution of global features at the expected Alfvén velocity time-scales. The setup complements our existing PXI setup that has 24 channels at 2.5 MS/s with another 96 channels at 50 MS/s 12 bits. The channels will be used for the magnetic probe array to reconstruct 3D magnetic fields necessary for helicity calculations. The digitizers are based on a combination of samplers and FPGAs to stream the data from analog inputs to onboard DRAM then to the PC. The FPGAs modules' primary advantage is the cost/channel while the downsides are the effort involved in programming these modules and non-linear response at low frequencies in the bandwidth (which are calibrated for in-house). This required considerable effort in addition to earlier 24 channel data acquisition with PXI-6133 modules. This work was performed by an excellent student supported on this award (Jens von der Linden), developing tremendous skill in FPGA programming using NI's LabView interface to program these digitizers and associate them with our existing setup. He is now a certified LabView instructor. The result is that we have 120 channels for data acquisition, all directly stored into the MDSplus database, and opto-electronic triggering channels for the whole experiment from a single LabView interface on the main PC control (Fig. 3).

Fig.14: (left) LabView control panel interface showing (1) timing sequencer, (2) time bar layout, (4) log input, (5) MDSplus data tree control; the LabView Control Panel was designed in-house and programmed to control the entire experiment charge-discharge-data acquisition & storage cycle; (middle) National Instruments FPGA data acquisition modules. Custom breakout boards to shielded CAT-7 ethernet panel mounts are not shown; (right) Programmable timing sequencer with 22 fast pulse optical triggers, or frequency modulation control signals, and 24 DC on/off optical outputs for relay switching. This allows complete, optically-isolated remote control of the entire experimental charge-hold-discharge cycle. The electro-optical converters and breakout boards were designed in-house to be a factor of 4 more power efficient.

Diagnostics

Magnetic probe array. Scheduled for completion April 2016. The probe array progress has been slow but steady due to graduate student performance (Manuel Azuara-Rosales, funded independently from this award). The probe array of 135 inductor chip coils (45 3D locations) was mounted in carrier tape inserted into a 6mm OD stainless steel tube (25% smaller than other experiments). The probe array is mounted on the chamber with a convenient, rotatable 3D printed mount designed by the student. Custom cables also made by the student convert the 138 BNC plugs to shielded ethernet plugs. The ethernet cables are plugged into an attenuator box connected to the data acquisition modules. The attenuators were designed by our group to have selectable attenuation between 0-76 dB with switchable pi-type balanced attenuators surface-mounted on PCB boards. To save cost, switches and mounts were made with our laboratory 3D printer. The probe is complete and undergoing calibration. Two more identical probe arrays were under construction but are put on hold.

Tomography spectroscopy. The fiber-bundle design is still being finalized and is currently on hold due to the effort re-focused on completing the power supplies, the plasma gun, the data acquisition and triggering system. The low-level software routines for 3D vector tomographic reconstruction has been ported with the help of undergraduate research students from IDL to C to improve reconstruction times by a factor of 10. The algorithm needs modification to include the exact viewchord locations of the experiment (it currently uses an approximate position coordinates) which will be determined in conjunction with the fiber-bundle design and chamber mounting characteristics. This work will be performed when the rest of the equipment has been commissioned when a student effort can be re-directed, after completion of construction of the new gas valves and power supplies. In the meantime, the 1m focal length monochromator will also be used for conventional single and dual-chord spectroscopy.

Other diagnostics. Rogowski coils, and high voltage probes have been successfully completed and tested/calibrated. We currently use Tektronix HV probes with a Tektronix oscilloscope and a custom solar-powered opto-isolated HV probe (circuit courtesy of Paul Bellan at Caltech). A He-Ne interferometer is near completion (project by graduate student Alexander Card). The interferometer works intermittently but

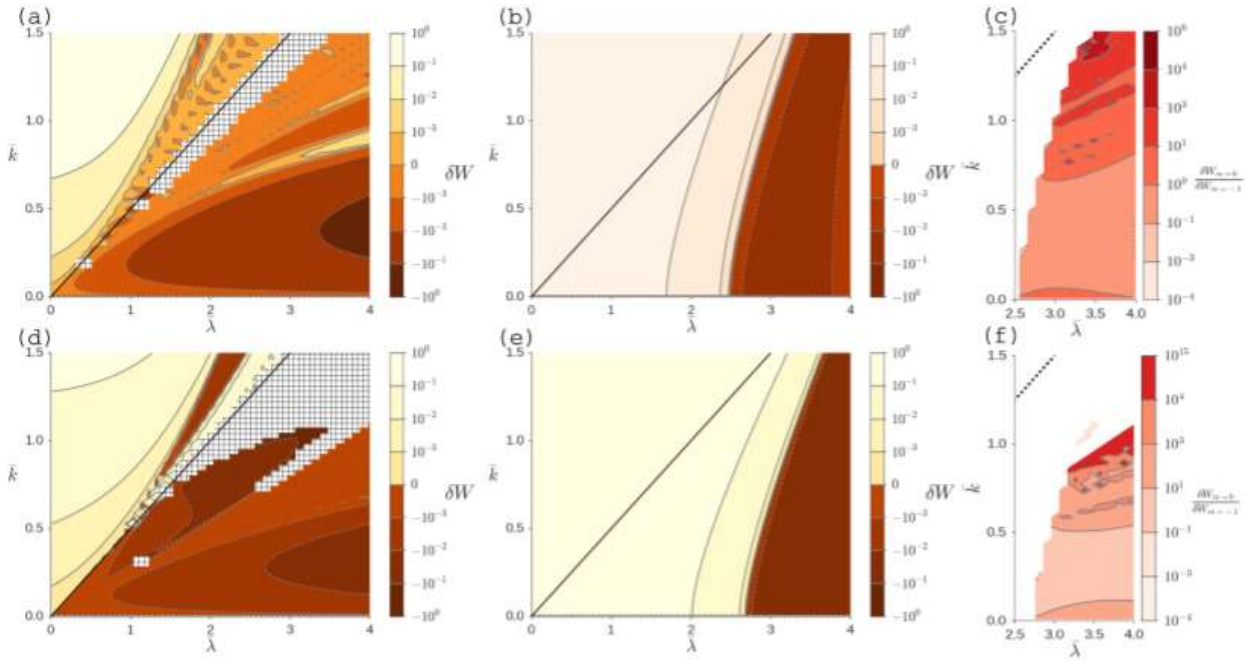

Fig. 15: Numerical stability space for kink (left column) and sausage (middle column) instabilities in a generalized current-carrying magnetic flux with core and skin currents. The horizontal axis is the current normalized to magnetic flux $\bar{\lambda} = \mu_0 Ia/\psi$ and tube radius. The vertical axis is the tube aspect-ratio $\bar{k} = 2\pi a/L$. Contours show the perturbed potential energy δW for the mode (light is stable with positive δW, dark is unstable with negative δW). The right column shows the ratio of the perturbed potential energies of sausage and kink modes. A short fat jet with low current begins life in the top-left stable region. An increasing current and lengthening jet travels to the bottom-right of the stability space crossing into the unstable regions, unstable to kink only at first then unstable to both kink and sausage simultaneously. The black straight diagonal line is the Kruskal-Shafranov condition.

is plagued by electronic noise. A Faraday cage and extra shielding is being designed by Alexander Card in parallel to his work on the data acquisition, plasma gun, and gas valves. A retarding grid energy analyzer was near completion during summer 2015 when the student (Morgan Quinley) decided to leave the university for employment after a MSAA and not pursue a PhD as previously planned. The energy analyzer was able to measure electron energies but not enough time was available to complete the project (modifying the electrodes stack setup for measuring ion energies).

Theory

Sausage instabilities on top of kinking lengthening current-carrying magnetic flux tubes (Fig. 15). We theoretically explored the possibility of sausage instabilities developing on top of a kink instability in lengthening current-carrying magnetic flux tubes. In the cosmos and terrestrial experiments, observations indicate that the dynamics of magnetic flux tubes can involve fast topological changes, and recent laboratory measurements suggest that hierarchies of instabilities such as kink and Rayleigh-Taylor could be responsible by locally accessing two-fluid and kinetic regimes. Sausage instabilities can also provide this coupling mechanism between disparate plasma scales. We have derived a single general criterion for the onset of both in idealized magnetic flux tubes carrying core and skin currents. The criterion indicates a dependence of stability boundaries in configuration space. Numerical investigations confirm the overlapping sausage and kink unstable regions with an inverse dependence on current profile inside the flux tube. The theoretical

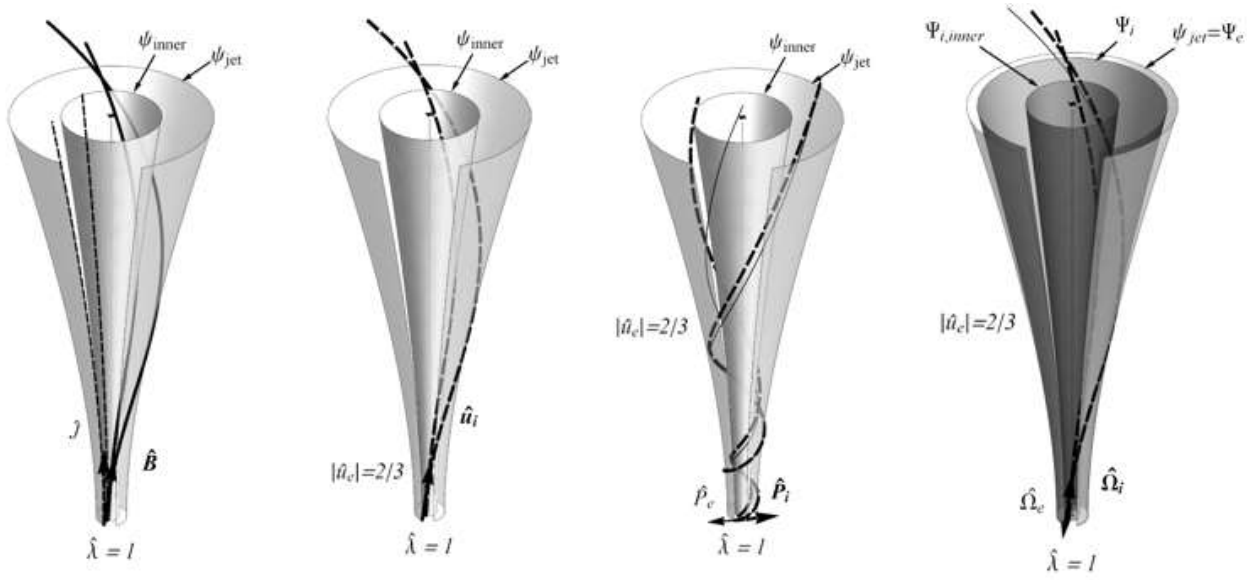

Fig. 16: Four equivalent visualizations of a flared current-carrying magnetic flux tube: (a) a jet defined by magnetic fields $\vec{B} = \nabla \times \vec{A}$ and current density showing two magnetic flux tubes ψ_{jet} and an inner core example ψ_{inner}; (b) the same jet with the same magnetic flux surfaces but showing the equivalent ion and electron flow fields (assuming massless electrons flowing at 2/3 magnetic Mach number; (c) the same jet with the same magnetic flux surfaces showing the equivalent canonical momentum field lines $\vec{P} = m\vec{u} + q\vec{A}$; (d) the same jet showing the same outer magnetic flux surface ψ_{jet} and also showing two flux surfaces $\psi_i = \int \vec{\Omega}_i \cdot d\vec{S}$ of ion canonical vorticity $\vec{\Omega}_i = \nabla \times \vec{P}_i$. The flux tubes of canonical vorticity (dark grey) are distinch and detached from the magnetic flux tube (light grey). Because the canonical vorticity is frozen-in to the plasma (generalized induction equation), the dark flux tubes are visible if plasma emits light, while the magnetic flux surfaces are invisible. For given current-profiles, the dark canonical flux tubes appear can collimate like astrophysical jet observations.

result has been presented at the APS DPP 2015 in Savannah, Georgia, at LLNL, and a manuscript is in preparation. The Mochi.LabJet experiment will measure the stability regions in this configuration space.

The topology of canonical flux tubes in flared jet geometry (Fig. 16). Magnetized plasma jets are generally modelled as magnetic flux tubes filled with flowing plasma governed by MHD. We have developed a more fundamental approach based on flux tubes of constant canonical vorticity, defined as the circulation of the species' canonical momentum. This approach extends the concept of magnetic flux tube evolution to include the effects of finite particle momentum and enables visualization of the topology of plasma jets in regimes beyond MHD. A flared, current-carrying magnetic flux tube in an ion-electron plasma with finite ion momentum is thus equivalent to a pair of electron and ion flow flux tubes, a pair of electron and ion canonical momentum flux tubes, or a pair of electron and ion canonical vorticity flux tubes. We have examined the kinematic evolution of all these flux tubes for increasing electrical currents, different radial current profiles, different electron Mach numbers, and a fixed, flared, axisymmetric magnetic geometry. Calculations of gauge-invariant relative canonical helicities track the evolution of magnetic, cross, and kinetic helicities in the system, and show that ion flow fields can unwind to compensate for an increasing magnetic twist. The results demonstrate that including a species' finite momentum can result in a very long collimated canonical vorticity flux tube even if the magnetic flux tube is flared. With finite momentum, density gradients are normal to canonical vorticities and not to magnetic fields, so observations of collimated astrophysical jets could be images of canonical vorticity flux tubes instead of magnetic flux tubes. A manuscript is in preparation. The software used to plot these plasma jets will also be useful for interpreting magnetic field and flow measurements in the Mochi.Labjet experiment.

A field theory approach to the evolution of canonical helicity and energy. A redefinition of the Lagrangian of a multi-particle system in fields reformulates the single-particle, kinetic, and fluid equations governing fluid and plasma dynamics as a single set of generalized Maxwell's equations and Ohm's law for canonical force-fields. The Lagrangian includes new terms representing the coupling between the motion of particle distributions, between distributions and electromagnetic fields, with relativistic contributions. The formulation shows that the concepts of self-organization and canonical helicity transport are applicable across single-particle, kinetic, and fluid regimes, at classical and relativistic scales. The theory gives the basis for comparing canonical helicity change to energy change in general systems. For example, in a fixed, isolated system subject to non-conservative forces, a species' canonical helicity changes less than total energy only if gradients in density or distribution function are shallow. This work lays the foundation for extending the quasi-static theory of flux tubes in fluid regimes to dynamics of canonical flux tubes in all regimes; it was presented as an invited talk at the mini-conference on coupling kinetic to fluid scales at the APS DPP 2015 in Savannah, Georgia; and has been submitted to Phys. Plasmas.

5.4. Year 4 (Apr 2016 – Apr 2017)

Experiment

Commissioning of the Mochi.LabJet experiment. The experiment achieved first plasma in Nov. 1, 2015. The commissioning phase of the hardware was nominally completed in Aug. 16, 2016 with a first operational campaign until Nov. 2016 to determine the first plasma parameters. This informed a small upgrade to the plasma gun that resulted in significant improvement in plasma lifetime (~10 μs to ~100 μs) during a second operational phase between Dec. 2016 and Mar. 2017. The commissioning included testing of all major power supplies, control hardware, and data acquisition. Three major issues were resolved:

1. The control and data acquisition equipment consists of off-the-shelf National Instruments timing and digitizer cards with custom opto-electronic transmitters and receivers, manipulated by a custom LabView PC graphical user interface (GUI). The data acquisition system has 128 digitizing channels, of which 96 channels are dedicated to magnetic (Bdot) probe arrays taking 40000 samples at 50 Ms/s with 12 bit resolution and 26 MHz bandwidth, made up of three NI-5752 analog-digital adapters mated to PXIe-7962R field-programmable array (FPGA) cards programmed in-house for control of the data streams. The next 24 digitizing channels take 2M samples at 2.5 Ms/s with 14 bit resolution at 1.3 MHz bandwidth, made up of three PXI-6133 cards housed in a PXI-1042Q chassis slaved to the PXIe-1082 chassis housing the FPGA boards. A pair of PXIe-6672 and PXI-6653 synchronization cards take care of overall synchronisation and communication to the PC. The remaining 8 channels are dedicated to HV probes for measuring gun voltages and outputs of a HeNe interferometer, made of two Tektronix 2024B digital storage oscilloscopes that take 2500 samples at 2 Gs/s with 200 Mhz bandwidth and remotely operated by a PC. The FPGA boards were programmed in house (by Jens von der Linden) who subsequently discovered that the NI-5752 digitizers had an undocumented resonance at 50 kHz and several other issues (centering of zero voltage, zero voltage level shifts, frequency dependent amplitudes). These issues were not known by National Instruments and after several rounds of communication between them and my students, they were finally resolved by applying software filters, careful characterization of the frequency

Fig. 17: Custom fast gas valves manufactured in house that can deliver 10^{21} particles each in 100 μs time scales. These valves are necessary for delivering sufficiently dense gas close to the electrodes for breakdown without having to pre-fill the vacuum chamber. This allows formation of dense plasma jets inside a vacuum and not inside a background gas.

response of the digitizers and a suggestion by Jens to the National Instruments engineers on programming the FPGAs. However, during testing of frequency response, a large amount of data stored in MDS+ were lost for reasons unclear. Backup images exist and the handwritten logs are still available but the stored current and voltage curves are lost (except in the images of oscilloscopes). Moving forward, we have implemented regular backups (local and to the cloud) and enforced any LabView development to occur on a separate MDS+ tree.

2. After unsatisfactory test results of commercial Parker valves (Series 9 and 99) for fast gas puffing into the chamber, it was decided to manufacture in house fast gas valves based on a design by Paul Bellan (Caltech) and Scott Hsu (LANL). Ten units were manufactured between Apr.-Jul. 2016 from raw materials by the students Evan Carroll and Alexander Card with painstaking precision and craftmanship (Fig. 17). The machining of stainless steel and the availability of access to the machine shop were the two major limiting factors for completing the task. A third student, Eric Sander Lavine, built a new ten channel pulsed power supply from spare parts to control the ten fast gas valves. The fast gas valves perform flawlessly and satisfactorily. The expenditure consisted mainly of raw materials (stainless steel and aluminum tubing), vacuum parts, small mechanical parts (springs, screws), and electrical/electronic parts (magnet wires, capacitors, resistors, connectors), for a total of \$2.5k or \$250 per unit, including the pulsed power supply.

3. During the first operational phase Aug.-Nov. 2016, arcing inside the chamber between the middle and outer electrodes during the discharge appeared to syphon significant current away from the main plasma jet. This resulted in a plasma jet lifetime of ~10 μs. The arcing occurred at two locations: in the gap between the two copper electrodes and between the re-entrant port and the vacuum chamber behind the electrodes. A new middle electrode with larger diameter was made to reduce the gap distance to be left of the Paschen curve. In addition, a cylindrical teflon sheet was inserted in the gap between the two electrodes, long enough to also cover the gap between the re-entrant port and the chamber. It successfully prevented arcing between the chamber and the port but did not

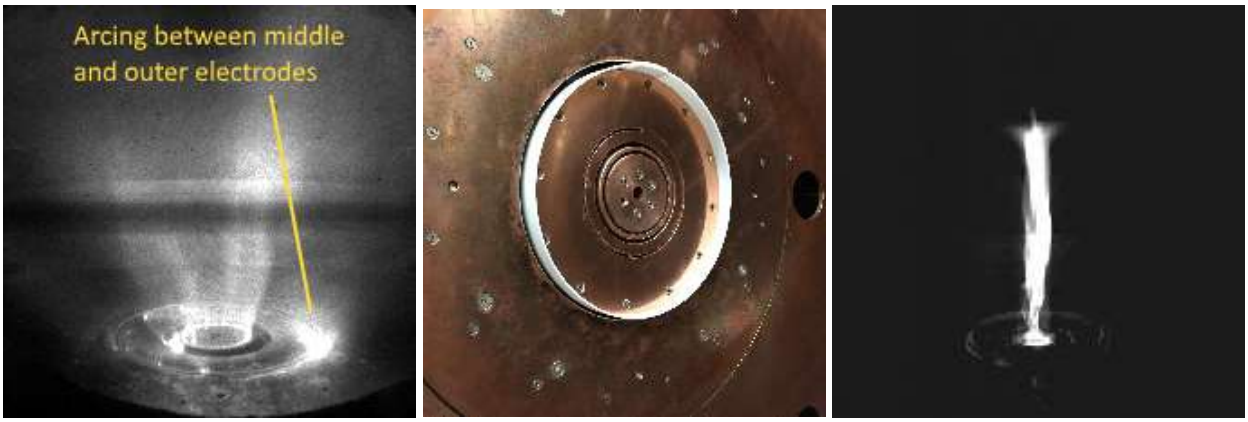

Fig. 18: (left) Typical image showing arcing between the middle and outer electrodes during the first operational phase. (middle) a new middle electrode and teflon insulating sheet was inserted to prevent the arcing resulting in (right) dense collimated jets ~30cm long that lasted ~10 μs before undergoing a kink instability and detaching (shot #6580).

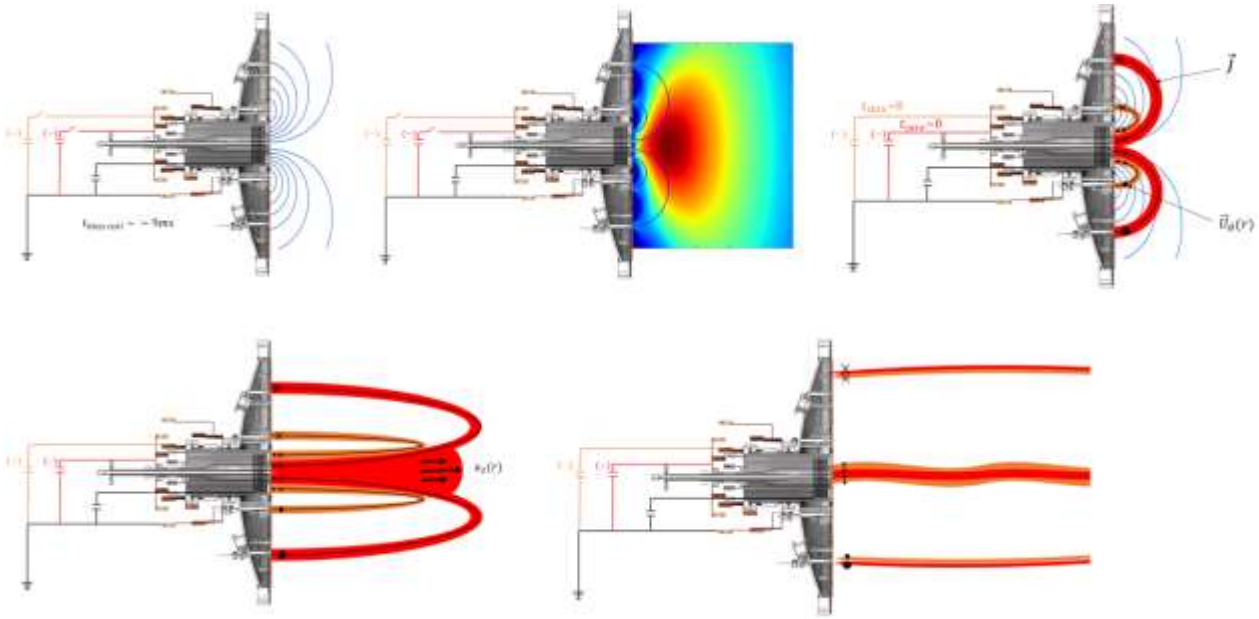

Fig.19: (top left to bottom right) Typical sequence for plasma discharge in Mochi.LabJet. A bias field is first applied; followed by gas puffs to form a dense cloud just in front of the electrodes (the rest of the vacuum chamber is at base vacuum pressure of 10^{-7} torr); bank discharges form the first plasma "bundt cake" shapes between the inner and outer electrodes (red "core") and between the middle and outer electrodes (orange "skin"); the plasma lengthens to form a jet that collimates, eventually going kink unstable and detaching, leaving the field of view.

improve the jet evolution much except added significant carbon impurities and a secondary plasma "bundt cake" around the teflon (Figs. 18, 22). The teflon appeared to have reduced arcing between the two electrodes but resulted in a plume similar to plumes from PPT thrusters (also based on teflon). We therefore designed an alumina insert for the gap between the plasma facing electrodes and the teflon sheet only served to prevent arcing between the chamber and the re-entrant port. This resulted in improved plasma jet lifetimes during the second operational phase between Dec. 2016-Mar. 2017. The expenditure was $1k.

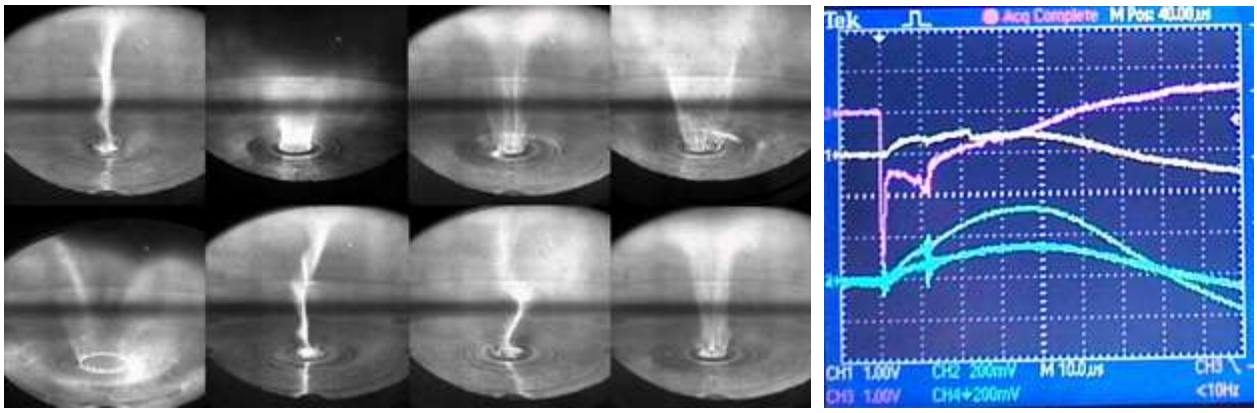

Fig. 19: (left) Shot 6200 series during the first operational phase Aug.-Nov. 2016. The hydrogen plasmas form dense collimated jets that lengthen to ~30 cm and go kink unstable. (right) Typical current (blue from core gun and green total from both core and skin guns) and voltage (yellow and purple) traces for the plasma discharge measured at the inner "core" gun and middle "skin" gun connectors. The typical voltages are -4 kV and currents are 120 kA.

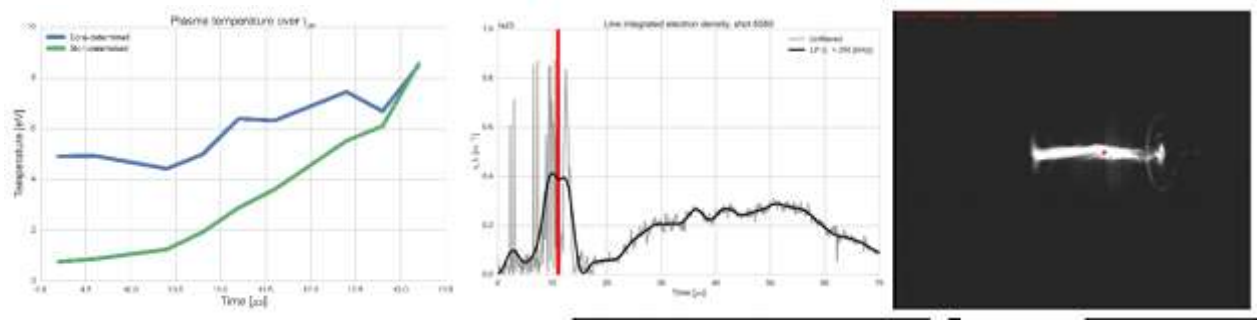

Fig. 20: Typical plasma parameters measured during the first operational campaign Aug.-Nov. 2016 (shot #6580): (left) plasma temperature estimated from Spitzer resistivity for the core plasma (blue) and the skin plasma (green) evolving during the jet life; (middle) the plasma line-integrated density measured with a HeNe interferometer over the discharge duration. The dense plasma jet exists in the 5-13 μs window. The red line indicates the time of the image (right) in which the red dot indicates the position of the HeNe laser scene beam at the axis of the chamber.

Operational phase 1 (Aug.-Nov. 2016), first plasma parameters (Figs. 18-20). The primary objective of the first operational phase was to characterize the plasma behavior and commission the primary diagnostics. After insertion of a teflon insulating sheet in the gap between the middle and outer electrodes, satisfactory collimated plasma jets formed and lasted ~10 μ]s. Figure 18 shows a typical sequence for a discharge and Figure 19 shows some sample images of the types of jets obtained. A vacuum poloidal magnetic field is generated 6 ms before the bank discharge and reaches a desired value at that time. Since the plasma lifetime is much shorter than the bias field RLC time, the vacuum bias magnetic field is considered constant. Gas is puffed 3-4 ms before the bank discharge and creates a dense cloud of gas in front of the electrodes. Because of our unique plenum design (azimuthally symmetric gas slits), the gas output is azimuthally symmetric and allows for plasma to rotate freely without anchoring to discrete gas holes. The banks are then discharged to form the plasma (one for each pair of electrodes: inner with outer for the "core" gun, and middle with outer for the "skin" gun). The initial plasma forms a "bundt cake" shape that expands out into the chamber to form a collimated dense magnetized jet that lengthens. The jet then usually goes kink unstable and detaches from the electrodes to dissappear from view.

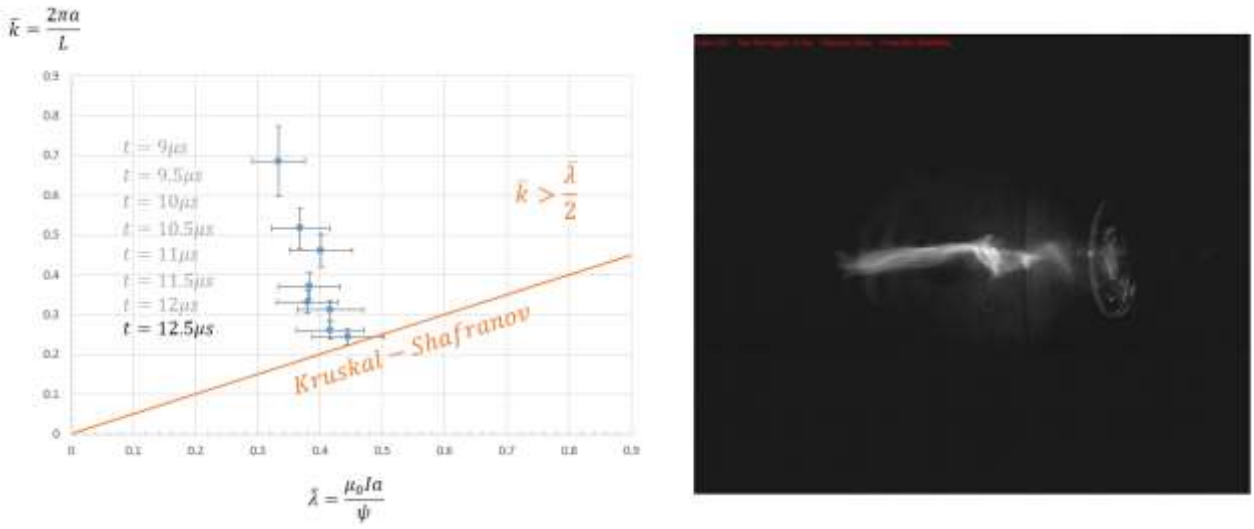

Fig. 21: (left) Evolution of jet in $k - \lambda$ space. The plasma starts short and thick (top left of the parameter space) and moves towards the bottom right of the space as it lengthens and current ramps up. It eventually crosses the kink instability Kruskal-Shafranov criterion; (right) image of the detached kinked jet at 12.5 μs.

The first diagnostics during this operation phase included high speed framing cameras (occasional use of a Kirana 50 million frames per second with 180 frames camera courtesy of the Univ. Washington Student Technology Fund, and a PiMAX 3 dual inline frame iCCD camera taken from our Doppler spectroscopy setup), a heterodyne unequal path length HeNe interferometer, gun currents and voltages. From the images, an axial jet velocity was estimated at 80 km/s. From interferometry (Fig. 20), the jet plasma density was ~1022 m-3. The magnetic field was estimated from Alfvén velocities or gun currents to be about 0.9 T (including the 0.3 T bias field strength). The temperature was estimated from Spitzer resistivity and current-voltages curves (Fig. 19) to start at ~1 eV for the skin of the jet and ~5 eV for the core of the jet, both rising to ~10 eV. The plasma jet lifetime from formation to detachment is about 5-10 μs.

The jet evolution can be characterized by the evolution of the dimensionless aspect ratio $\bar{k} = 2\pi a/L$ with respect to the dimensionless current $\bar{\lambda} = \mu_0 I a/\psi$ (where a is the jet radius, L is the jet length, I is the total current carried in the jet, and ψ is the total magnetic flux). In this parameter space (Fig. 6), the jet evolves from the top-left (short and thick at low currents) to the bottom right (long and thin at high currents) and goes kink unstable as expected at the classical Kruskal-Shafranov threshold ($\bar{k} = \bar{\lambda}/2$).

After the collimated jet, the discharge continues with a tenuous plasma that has no distinguishing features except for a glow around the teflon sheet and a thick plume of plasma resembling a PPT thruster. The gun currents and voltages have under-damped RLC half cycles of 70 μs or more, suggesting that significant electrical power would still be available to drive a plasma jet if it could be prevented from driving the teflon glow. We therefore designed and purchased an alumina insert to replace the teflon sheet (Dec. 2016).

A manuscript describing the Mochi.LabJet experiment and the first plasma results is in preparation. The progress was reported at the APS DPP meeting in Nov. 2016 in San Jose, CA (three posters, one talk).

Operational phase 2 (Dec. 2016 – Mar. 2017), plasma improvements (Figs. 22-23). The alumina insert significantly improves the plasma evolution by preventing any arcing in the gap between electrodes that appeared to syphon off current away from the main jet. The discharge duration now exhibits three distinct

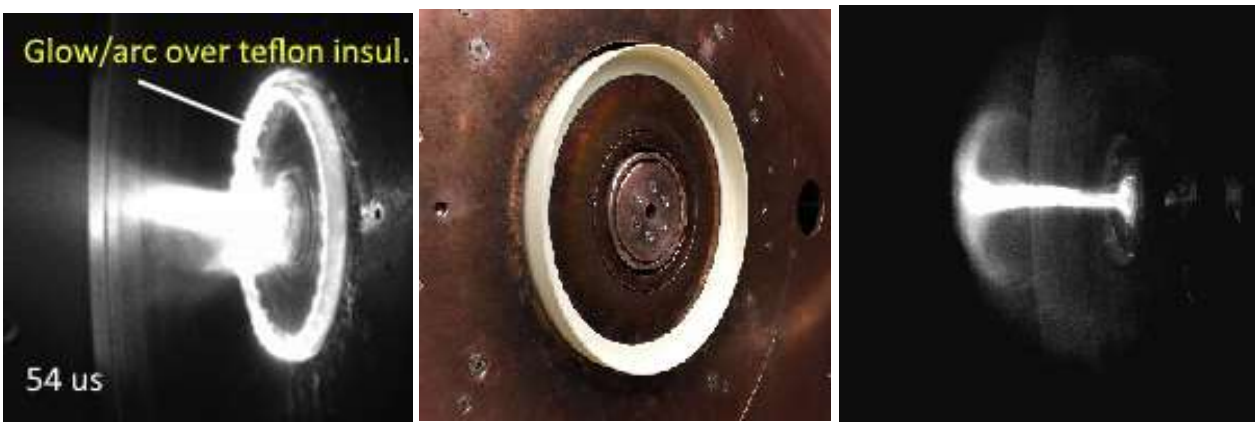

Fig. 22: (left) glowing arc over the teflon insulator after the plasma jet detaches. The bank continues to power the discharge for another 50 μs but only the glow and a faint diffuse plume is visible; (middle) alumina insert designed to replace the teflon and prevent arcing; (right) image of the plasma jet after the alumina insert in position. The jet behaves similarly to the first campaign but following the detachment, a second, longer lasting jet forms (Fig. 8).

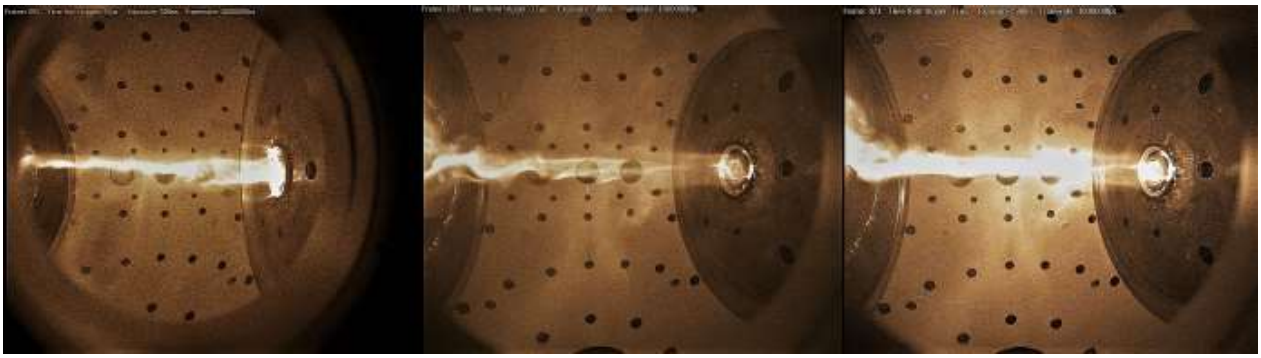

Fig. 23: Typical plasmas from two different discharges of the second operational campaign (left shot #6874, middle and right #6906, -5.2kV on skin gun and -6.1 kV on core gun, 160 kA total current, Dec. 2016-Mar. 2017). The magnetized plasma jets are ~1.1m long with significant currents and helical flows, reaching the other end of the chamber (the opposite end are floating surfaces, i.e. not electrically connected to the vacuum chamber nor any power supply).

periods: the first period is similar to the first operational campaign with a short-lived, dense plasma jet that rapidly collimates, goes kink unstable and detaches; the second period begins a formation of a second plasma jet that expands with little collimation; the third period involves collimation of this second plasma jet into a large aspect-ratio jet with significant currents and significant helical flows that appear to stabilize the jet to kink instabilities. The plasma jet is ~1.1m long carrying 160-200 kA currents and lasting ~50 μs (about 40-50 Alfvén times).

Analysis of the trajectory in $\bar{k} - \bar{\lambda}$ space (Fig. 24) confirms that the first plasma jet behaves similarly to those in the first campaign with a short thick jet that collimates, lengthens, goes kink unstable then detaches (green curve, 11-15 μs, with $\bar{k} < 0.4$ and $\bar{\lambda} < 0.3$, Fig. 24). The second plasma jet begins short and thick at a significantly larger inverse aspect-ratio $\bar{k} > 0.8$, with current rising to bring the jet into the kink unstable region (blue curve, 21-45 μs) yet remaining stable. The jet has a large aspect-ratio ($\bar{k} < 0.15$), is stable to kink instabilities even as current decreases in the kink unstable region (orange curve, 50-90 μs). The stable jets are correlated with significant helical flows while instabilities are correlated with the absence of such

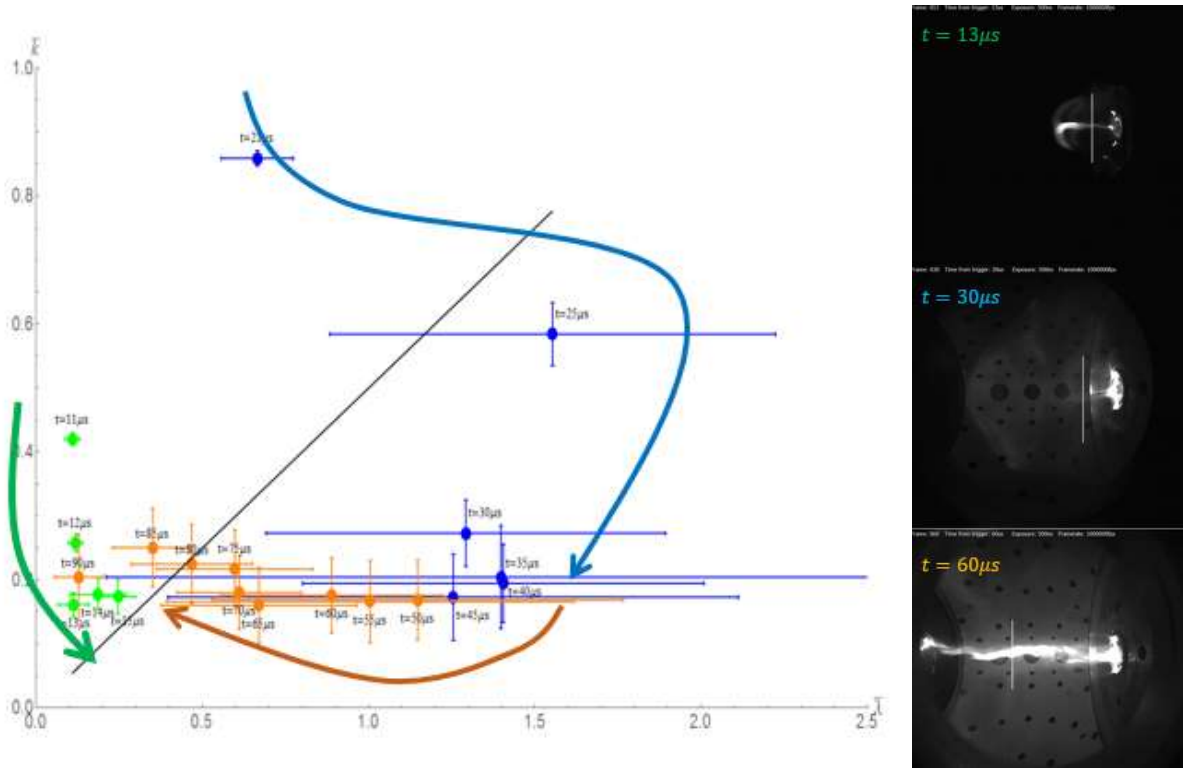

Fig. 24: Typical plasma evolution in stability space during the second operational campaign (Dec. 2016-Mar.2017): (left) three time periods are observed during the full discharge. The initial dense jet behaves similarly to the first operational campaign (green), followed by a new second jet that forms short and thick (blue) and expands into kink unstable region (black solid line) as current ramps up. This jet then collimates and lengthens to reach the chamber end at 1.1m while remaining stable even deep inside the kink unstable parameter space region; (right column) images of the plasma during the three time periods, showing the first jet (top right), the second jet at formation (middle right) and the straight stable jet with flows (bottom right).

flows. Flows are observed with Doppler spectroscopy and preliminary data suggests azimuthal flows of a 2-7 km/s with axial flows of 30-80 km/s.

We are in the process of confirming the numbers and a manuscript describing these remarkable results is in preparation.

Diagnostics

He-Ne interferometer. The interferometer is operational. The diagnostic was built by Alexander Card and provides density data on a regular basis. The earlier issues with electronic noise were mostly solved by using an independent oscilloscope to digitize the signals instead of the main digitizers. Issues with background amplitude variations in signals are resolved with software low-pass filters.

Magnetic probe arrays. Three arrays are operational since Jan. 2017 with final (re)calibration in Mar. 2017. We have a limited number of digitizer channels (120 channels) but can choose which coils to measure out of the 405 total. They were built by Manuel Azuara-Rosales (funded independently from this award). Each probe array of 135 inductor chip coils (45 3D locations) are mounted in carrier tape inserted into a 6mm OD stainless steel tube (25% smaller than other experiments) sheathed within a 8mm OD alumina tube. The probe arrays are mounted on the chamber with a convenient, rotatable 3D printed mount designed by the student. Custom cables also made by the student convert the 138 BNC plugs to shielded ethernet plugs. The

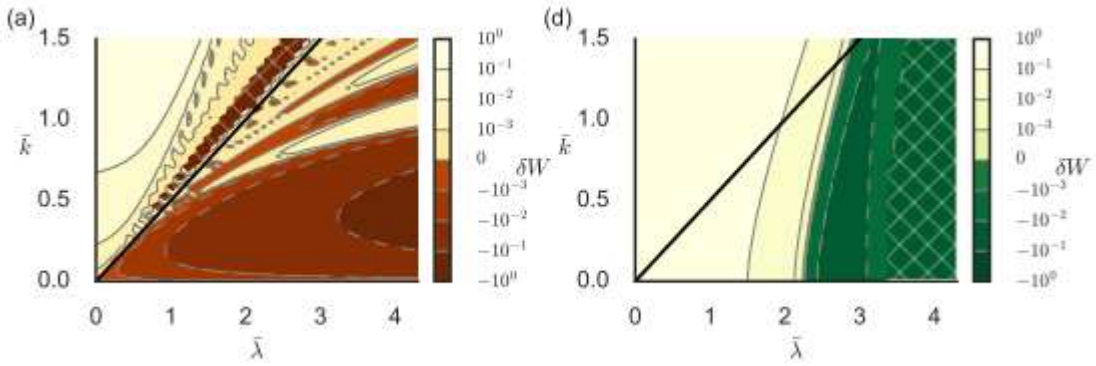

Fig. 25: Numerical $\bar{k} - \bar{\lambda}$ stability spaces with relative growth rates. (a) Normalized kink δWm=1 contours for ϵ_{eff}= 0.7; (d) Normalized sausage δWm=0 contours for ϵ_{eff} = 0.7. The cross hatched regions indicate Suydam unstable regions in the m = 1 plots and regions with internal instabilities in the m = 0 plots.

ethernet cables are plugged into an attenuator box connected to the data acquisition modules. The attenuators were designed by our group to have selectable attenuation between 0-76 dB with switchable pi-type balanced attenuators surface-mounted on PCB boards. To save cost, switches and mounts were made with our laboratory 3D printer. Preliminary data confirm the strength of current-driven magnetic fields to be ~0.5 T and time-of-flight axial velocities of 50-80 km/s.

Tomography spectroscopy. The fiber-bundle design has been finalized and is being built in house by Eric Sander Lavine after a successful prototype and should be completed by mid April 2017. The low-level software routines for 3D vector tomographic reconstruction has been ported with the help of undergraduate research students from IDL to C to improve reconstruction times by a factor of 10. The algorithm needs modification to include the exact viewchord locations of the experiment (it currently uses an approximate position coordinates) which will be determined in conjunction with the fiber-bundle design and chamber mounting characteristics. We expect to obtain the first multi-chord spectroscopic data in the third operational campaign planned for Apr-June 2017.

Theory

Sausage instabilities on top of kinking lengthening current-carrying magnetic flux tubes (accepted and in print, Phys. Plasmas, Mar. 2017). We theoretically explored the possibility of sausage instabilities developing on top of a kink instability in lengthening current-carrying magnetic flux tubes. In the cosmos and terrestrial experiments, observations indicate that the dynamics of magnetic flux tubes can involve fast topological changes, and recent laboratory measurements suggest that hierarchies of instabilities such as kink and Rayleigh-Taylor could be responsible by locally accessing two-fluid and kinetic regimes. Sausage instabilities can also provide this coupling mechanism between disparate plasma scales. We have derived a single general criterion for the onset of both in idealized magnetic flux tubes carrying core and skin currents. The criterion indicates a dependence of stability boundaries in configuration space. Numerical investigations confirm the overlapping sausage and kink unstable regions with an inverse dependence on current profile inside the flux tube. The Mochi.LabJet experiment has begun to measure the stability regions in this configuration space (Figs. 21, 24 and 25).

The topology of canonical flux tubes in flared jet geometry (published, Astrophys. J., 835:89, Jan. 2017). Magnetized plasma jets are generally modelled as magnetic flux tubes filled with flowing plasma

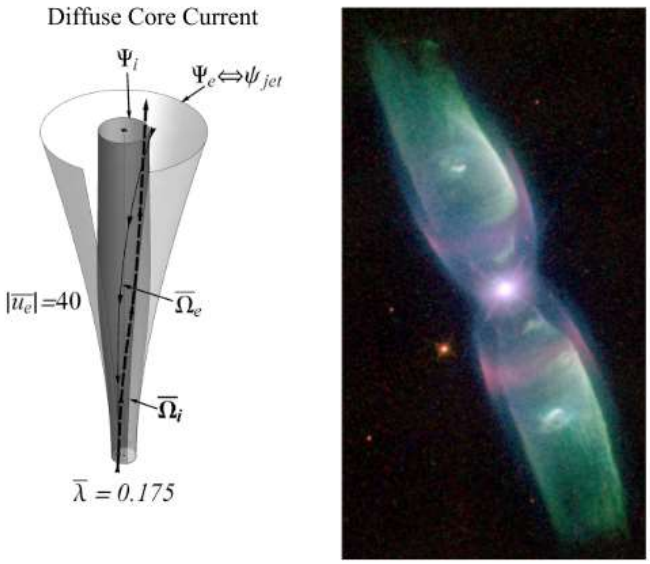

Fig. 26: (Left) Bulged ion canonical vorticity flux tube Ψi (dark gray) for a diffuse core current jet with low current (λ = 0.175) and a large electron velocity (| u_e | = 40). Equation (5) shows that density gradients can be normal to the dark gray canonical Ψi surfaces rather than the light gray magnetic flux surfaces ψ suggesting that ion line emission reveals canonical flux tubes as opposed to magnetic flux tubes. (Right) M2-9 Butterfly nebula (NASA HSTSTIS/CCD—MIRVIS),a bipolar planetary nebula with distinctive bulging that resembles the ion canonical flux tube in the left panel. Transitions in the geometry of the jet (i.e., flaring to collimation) may therefore also reflect changes in the relative strength of the fluid flow vorticity flux to the magnetic flux. Image credit: Bruce Balick (University of Washington), Vincent Icke (Leiden University), Garret Mellema (Stockholm University), and NASA.

governed by MHD. We have developed a more fundamental approach based on flux tubes of constant canonical vorticity, defined as the circulation of the species' canonical momentum. This approach extends the concept of magnetic flux tube evolution to include the effects of finite particle momentum and enables visualization of the topology of plasma jets in regimes beyond MHD. A flared, current-carrying magnetic flux tube in an ion-electron plasma with finite ion momentum is thus equivalent to a pair of electron and ion flow flux tubes, a pair of electron and ion canonical momentum flux tubes, or a pair of electron and ion canonical vorticity flux tubes. We have examined the kinematic evolution of all these flux tubes for increasing electrical currents, different radial current profiles, different electron Mach numbers, and a fixed, flared, axisymmetric magnetic geometry. Calculations of gauge-invariant relative canonical helicities track the evolution of magnetic, cross, and kinetic helicities in the system, and show that ion flow fields can unwind to compensate for an increasing magnetic twist. The results demonstrate that including a species' finite momentum can result in a very long collimated canonical vorticity flux tube even if the magnetic flux tube is flared. With finite momentum, density gradients are normal to canonical vorticities and not to magnetic fields, so observations of collimated astrophysical jets could be images of canonical vorticity flux tubes instead of magnetic flux tubes. The software used to plot these plasma jets will also be useful for interpreting magnetic field and flow measurements in the Mochi.Labjet experiment.

A field theory approach to the evolution of canonical helicity and energy (published, Phys. Plasmas, 23, 072108, July 2016). A redefinition of the Lagrangian of a multi-particle system in fields reformulates the single-particle, kinetic, and fluid equations governing fluid and plasma dynamics as a single set of generalized Maxwell's equations and Ohm's law for canonical force-fields. The Lagrangian includes new terms representing the coupling between the motion of particle distributions, between distributions and electromagnetic fields, with relativistic contributions. The formulation shows that the concepts of self-

organization and canonical helicity transport are applicable across single-particle, kinetic, and fluid regimes, at classical and relativistic scales. The theory gives the basis for comparing canonical helicity change to energy change in general systems. For example, in a fixed, isolated system subject to non-conservative forces, a species' canonical helicity changes less than total energy only if gradients in density or distribution function are shallow. This work lays the foundation for extending the quasi-static theory of flux tubes in fluid regimes to dynamics of canonical flux tubes in all regimes; it was presented as invited talks at EPFL (Lausanne, Switzerland), ESA (ESTEC, Noordwijk), Univ. Pierre et Marie Curie (Paris, France) and at the APS DPP 2016 in San Jose, CA.

5.5. End of Year 4 (Apr 2017 – Jun 2017)

The project concentrated exclusively on the third operational campaign, which is the only operational campaign to have the complete set of diagnostics: current, voltages, interferometer, magnetic probe arrays and ion Doppler spectroscopy. The project was terminated on July 15th, 2017. The PI and last remaining student have been analysing the data and writing up the results, supported by personal funds.

6. Products developed under the award

6.1. Publications.

1. J. von der Linden, S. You, *''Sausage instabilities on top of kinking lengthening current-carrying magnetic flux tubes"*, Phys. Plasmas, **24**, 052105 (2017) doi: 10.1063/1.4981231.
2. E. S. Lavine, S. You, "*The topology of canonical flux tubes in flared jet geometry*", Astrophys. J., **835**:89 (2017) DOI:10.3847/1538-4357/835/1/89
3. S. You, "*A field theory approach to the evolution of canonical helicity and energy*", Phys. Plasmas., **23**, 072108 (2016) DOI:10.1063/1.4956465
4. S. You, *"A two-fluid helicity transport model for flux-rope merging"*, Plasma Phys. Control. Fusion, **56**, 064007 (2014) DOI: 10.1088/0741-3335/56/6/064007
5. H. Tanabe, H. Oka, M. Annoura, A. Kuwahata, K. Kadowaki, Y. Kaminou, S. You, A. Balandin, M. Inomoto and Y. Ono, *"Two-dimensional imaging measurement of magnetic reconnection outflow in the TS-4 toroidal plasma merging experiment"*, Plasma and Fusion Research, **8**, 2405088 (2013) DOI: 10.1585/pfr.8.2405088
6. H. Tanabe, A. Kuwahata, H. Oka, M. Annoura, H. Koike, K. Nishida, S. You, Y. Narushima, A. Balandin, M. Inomoto, Y. Ono, *"Two-dimensional ion temperature by application of tomographic reconstruction to Doppler spectroscopy"*, Nucl. Fusion, **53**, (2013) 093027 DOI: 10.1088/0029-5515/53/9/093027
7. S. You, *"The transport of relative canonical helicity"*, Phys. Plasmas, **19**, 092107 (2012) DOI: 10.1063/1.4752215

6.2. Pending publications

Pre-prints will be uploaded to arXiv.

1. S. You, J. von der Linden, E. S. Lavine, E. G. Carroll, A. Card, M. Quinley, M. Azuara-Rosales, *"The Mochi.LabJet experiment for measurements of canonical helicity injection in a laboratory astrophysical jet"*, subm. Ap. J. Supl. Ser., (2017) https://arxiv.org/abs/1711.07213
2. E. S. Lavine, S. You, *"Helical shear flow stabilization of a laboratory astrophysical jet"*, in prep.
3. J. von der Linden, J. Sears, T. Intrator, S. You, *"Measurements of the canonical helicity of a gyrating kink"*, in prep.
4. Y. Kamikawa, S. You, *"Analysis of plasma detachment in a magnetic nozzle with canonical field theory"*, in prep.
5. E. S. Lavine, S. You, *"Double-helix state observed in the Mochi.LabJet experiment"*, in prep.

6.3. Conference papers.

2016

1. You S, von der Linden J, Lavine ES, Card A, Carroll E, ''The Mochi Project: a field theory approach to plasma dynamics and self-organization'', American Physical Society, Division of Plasma Physics (58th APS DPP 2016, San Jose, California).

2. Von der Linden J, Sears J, Intrator T, You S, ‘’Investigating the dynamics of canonical flux tubes’’, American Physical Society, Division of Plasma Physics (58th APS DPP 2016, San Jose, California).
3. Lavine ES, You S, ‘’The topology of canonical flux tubes in flared jet geometry’’, American Physical Society, Division of Plasma Physics (58th APS DPP 2016, San Jose, California).
4. You S, “A field theory approach to plasma self-organization”, US-Japan CT Workshop (USJCTW 2016, Irvine, California).
5. Von der Linden J, You S, “Investigating the dynamics of canonical flux tubes”, US-Japan CT Workshop (USJCTW 2016, Irvine, California).

2015

1. You S, von der Linden J, Vereen K, Lavine ES, Card A, Azuara-Rosales M, Quinley M, Yun GS, “Experimental and theoretical developments in the Mochi project”, American Physical Society, Division of Plasma Physics (57th APS DPP 2015, Savannah, Georgia).
2. You S, “Canonical field theory”, American Physical Society, Division of Plasma Physics (57th APS DPP 2015, Savannah, Georgia).
3. Von der Linden J, You S, “Sausage instabilities on top of kinking lengthening current-carrying magnetic flux tubes”, American Physical Society, Division of Plasma Physics (57th APS DPP 2015, Savannah, Georgia).
4. Sieck P, Woodruff S, Stuber J, Romero-Talamas C, Rivera W, You S, Card A, “Additive manufacture (3D printing) of plasma diagnostic components and assemblies for fusion experiments”, American Physical Society, Division of Plasma Physics (57th APS DPP 2015, Savannah, Georgia).
5. You S, ‘’Canonical helicity transport in turbulent magnetized plasmas’’, Basic Plasma Science User Facility Workshop (BaPSF 2016, Los Angeles, California).

2014

1. Von der Linden J, You S, “Dynamics of Laboratory Astrophysical Jets with Magnetized Helical Flows”, American Physical Society, Division of Plasma Physics (56th APS DPP 2015, New Orleans, Louisiana).
2. Carrol E, von der Linden J, Quinley M, You S, “Optically Isolated Control of the MOCHI Labjet High Power Pulsed Plasma Experiment”, American Physical Society, Division of Plasma Physics (56th APS DPP 2015, New Orleans, Louisiana).
3. Azuara-Rosales M, You S, “High-Resolution B-Dot Probe for Measuring 3D Magnetic Field in the MOCHI Labjet Experiment”, American Physical Society, Division of Plasma Physics (56th APS DPP 2015, New Orleans, Louisiana).
4. Card A, Vereen K, You S, “Optical Diagnostics in the MOCHI Labjet Experiment”, American Physical Society, Division of Plasma Physics (56th APS DPP 2015, New Orleans, Louisiana).
5. Lavine ES, You S, “Investigating the Dynamics of Canonical Flux Tubes in Jet Geometry”, American Physical Society, Division of Plasma Physics (56th APS DPP 2015, New Orleans, Louisiana).
6. Lavine ES, von der Linden J, Vereen K, Carroll E, Azuara-Rosales M, Card A, Quinley M, Datta I, You S, “Dynamics of Laboratory Astrophysical Jets with Magnetized Helical Flows”, American Physical Society, Pacific Northwest Section (15th APS PNW 2014, Seattle, Washington).

2013

1. You S, von der Linden J, Vereen K, Carroll E, Lavine ES, "A Laboratory Astrophysical Jet to Study Canonical Flux Tubes", American Physical Society, Division of Plasma Physics (56th APS DPP 2013, Denver, Colorado).
2. von der Linden J, Vereen K, Carroll E, Lavine ES, You S, "Investigating the Dynamics of Canonical Flux Tubes", American Physical Society, Division of Plasma Physics (56th APS DPP 2013, Denver, Colorado).
3. Vereen K, You S, "Vector Tomographic Reconstruction of 3D Plasma Flows with Ion Doppler Spectroscopy", American Physical Society, Division of Plasma Physics (56th APS DPP 2013, Denver, Colorado).
4. Lavine ES, You S, "Development of Fast Ion Gauge for Time-Resolved Neutral Gas Density Measurements", American Physical Society, Division of Plasma Physics (56th APS DPP 2013, Denver, Colorado)
5. Carroll E, You S, "A Modular, IGBT Driven, Ignitron Switched, Optically Controlled Power Supply", American Physical Society, Division of Plasma Physics (56th APS DPP 2013, Denver, Colorado).
6. Kamikawa Y, von der Linden J, Vereen K, Carroll E, Lavine ES, You S, "Test, Construction, and Calibration of a Fast Valve Driver Unit (FVDU) and an Earth-isolated High Voltage Probe (HV probe) for a pulsed plasma experiment", American Physical Society, Division of Plasma Physics (56th APS DPP 2013, Denver, Colorado).
7. Tanabe H, Kuwahata A, Yamada T, Watanabe T, Gi K, Annoura M, Kadowaki K, Kaminou Y, Koike H, Nishida K, Inomoto M, You S, Crowley B, Conway N, Scannel R, Gryaznevich M, Ono Y, "Study of Local Plasma Heating during Magnetic Reconnection by Tomographic Ion Doppler Spectroscopy in TS-3, TS-4 and MAST", American Physical Society, Division of Plasma Physics (56th APS DPP 2013, Denver, Colorado).
8. You S, "A two-fluid helicity transport model to explain bifurcation in counter-helicity merging", Workshop on Exploratory Topics in Plasma and Fusion Research (7th EPR 2013, Fort Worth, Texas).
9. You S, "A two-fluid helicity transport model to explain bifurcation in counter-helicity mergning", Workshop on Interrelationship between Plasmas in Laboratory and Space (IPELS 2013, Hakuba, Japan).

6.4. Student Dissertations

Available online at UW Library website: http://www.lib.washington.edu/engineering/resources/theses

1. J. von der Linden, "Investigating the dynamics of canonical flux tubes", Ph. D. Dissertation, University of Washington, (2017)
2. Y. Takagaki, "Analysis of plasma detachment through a magnetic nozzle via canonical field theory", M. S. A. A. Dissertation, University of Washington, (2017)
3. A. H. Card, "Implementation of an unequal path length, heterodyne interferometer on the Mochi.LabJet experiment", M. S. A. A. Dissertation, University of Washington, (2017)
4. E. G. Carroll, "Driving flows in laboratory astrophysical plasma jets: the Mochi.LabJet experiment", M. S. A. A. Dissertation, University of Washington, (2016)
5. M. Quinley, "Development of a gridded energy analyzer for measurement of the Mochi experiment ion energy distribution", M. S. A. A. Dissertation, University of Washington, (2015)

Pending

6. E. S. Lavine, Ph. D. Dissertation, University of Washington, (pending 2018)

6.5. Other public releases and websites

- Scientia public outreach article: “Professor Setthivoine You – Hope for Humanity in the Energy Crisis: Astronomical Jets in a Lab”, Dec. 2017, https://doi.org/10.26320/SCIENTIA63
- Interview for a general public outreach article in *Science et Vie* magazine on fusion rockets, Science & Vie, issue 1179, Nov. 2015 (web link)
- Seminar on « Exploiting plasma self-organization for fusion energy concepts » for the « American Institute for Aeronautics and Astronautics » (AIAA) meeting of Pacific NW, Paine Field, WA, 2015
- Vidéo for Microsoft using the Surface tablet and pen for research and teaching (https://www.youtube.com/watch?v=owf93l1YkOs), 2015
- MDC Vacuum Corporation, web article on the construction of the spherical vacuum chamber: https://www.mdcvacuum.com/DisplayContentPageFull.aspx?cc=MDC_SPHERICAL_UHV_CHAMBER, 2016

6.6. Networks or collaborations fostered

- RSX group, Los Alamos National Laboratory: before passing away, Tom Intrator and the PI discussed applying the canonical field theory analysis to the massive dataset of RSX, one of the only experiments with full 3D flow measurements necessary for determining canonical helicity. The collaboration was carried out this last year with J. Sears, a former postdoc of T. Intrator on RSX, now at Lawrence Livermore National Laboratory.
- Ono group, Univ. Tokyo, Japan: the collaboration with Y. Ono and H. Tanabe consists of developing ion flow diagnostics with multichord spectroscopy and vector tomographic reconstruction, and analysing data from merging-reconnection of compact toroids with canonical field theory.
- G. S. Yun, Pohang Institute of Technology (Postech), South Korea: networking with the beginning of a collaboration. G. S. Yun temporarilly provided a RF spectrometer to observed ion cyclotron emission from the Mochi.LabJet plasmas.
- S. Mazouffre, Laboratoire ICARE, Centre National de la Recherche Scientifique (CNRS), Orléans, France: networking with collaboration discussions on magnetic nozzles coupled to Hall thrusters.

6.7. Databases, software, educational aid or curricula

See appendixes in J. von der Linden Ph. D. thesis for details [Products 6.4.1] on the following software:

- Fluxtube stability code
- Mochi.Control and Mochi.FPGAControl codes
- Canonical flux tube and helicity reconstruction code